Calhoun
Institutional Archive of the Naval Postgraduate School

Calhoun: The NPS Institutional Archive

DSpace Repository

Theses and Dissertations 1. Thesis and Dissertation Collection, all items

1970

An investigation of biaxial stress in rubber modified plastics.

Oien, Harley Martin

Massachusetts Institute of Technology

http://hdl.handle.net/10945/15048

Downloaded from NPS Archive: Calhoun

DUDLEY
KNOX
LIBRARY

Calhoun is the Naval Postgraduate School's public access digital repository for research materials and institutional publications created by the NPS community. Calhoun is named for Professor of Mathematics Guy K. Calhoun, NPS's first appointed -- and published -- scholarly author.

Dudley Knox Library / Naval Postgraduate School
411 Dyer Road / 1 University Circle
Monterey, California USA 93943

http://www.nps.edu/library

AN INVESTIGATION OF BIAXIAL STRESS IN RUBBER MODIFIED PLASTICS

Harley Martin Oien

AN INVESTIGATION OF BIAXIAL STRESS IN RUBBER MODIFIED PLASTICS

by

HARLEY MARTIN OIEN

A.B., State University of South Dakota

(1962)

Submitted in Partial Fulfillment of the Requirements
for the Degrees of Naval Engineer and Master of Science
in Naval Architecture and Marine Engineering

at the

MASSACHUSETTS INSTITUTE OF TECHNOLOGY

(June 1970)

ARY
AL POSTGRADUATE SCHOOL
TEREY, CALIF. 93940

ABSTRACT

AN INVESTIGATION OF BIAXIAL STRESS IN RUBBER MODIFIED PLASTICS

by

HARLEY MARTIN OIEN

Submitted to the Department of Naval Architecture and Marine Engineering on June 4, 1970, in partial fulfillment of the requirements for the degree of Naval Engineer and Master of Science in Naval Architecture and Marine Engineering.

Thermosetting plastic materials consisting of EPON 828 monomer modified with 10% by weight of various Acrylonitrile/Butadiene copolymers were cast in flat plate and cylindrical molds and cured with Curing Agent D. Three series of materials were investigated: EPON 828 (unmodified), EPON 828 modified with CTBN R-146 (small particles) and EPON 828 modified with CTBN R-151N (large particles).

Cantilever and biaxial specimens for each of the series were tested at room temperature to determine fracture surface energy and biaxial stress yielding envelopes.

EPON 828 (unmodified) and CTBN R-146 materials displayed low fracture toughness, Von Mises Criterion yielding envelopes and an absence of stress whitening, whereas CTBN R-151N materials exhibited greatly increased fracture toughness, a cusp shaped yield curve and large amounts of stress whitening in both cantilever and biaxially tested specimens.

Optical and electron scanning micrographs of fractured and stressed materials revealed a marked difference in specimen morphology. The large elastomer particles of CTBN R-151N cleavage surfaces were surrounded by matrix material which was plastically strained, forming a porous surface believed to be created by the triaxial stress at the tip of the crack. Annealing of this surface relaxed the material, destroying porosity and exposing small particles, calculated to be elastomer particles.

Micrographs of biaxial specimens of CTBN R-151N showed large amounts of stress whitening, voids and an elongation of elastomer particle sites in a direction perpendicular to the tensile axis. Particle sites further exhibited band type structure emanating from their tips at small angles to the particle site major axis.

It is concluded that when stressed within a biaxial stress field a threshold of elastomer particle size exists above which fracture toughness is greatly increased, stress whitening occurs, the biaxial stress yield envelope is cusp shaped and large shear forces are created with resultant elastomer particle site deformation, band formation and creation of voids within the material.

Thesis Supervisor: Frederick J. McGarry
Title: Professor, Department of Civil Engineering

ACKNOWLEDGMENTS

I wish to gratefully acknowledge the concern and assistance afforded me in the work related to this investigation. My thesis supervisor, Professor F. J. McGarry, kindled an interest in these materials and offered many helpful suggestions and data interpretations. Professor Jacques Sultan, without whose help I could not have accomplished the optical and electron scanning microscopy and its subsequent data interpretation. Mr. Arthur Rudolph, Materials Division machinist, whose trust, patience and watchful eye contributed to achievement of highest quality obtainable in specimen machining.

Finally I wish to dedicate this work to that person most responsible for nurturing my education, the sunshine of "Smile Hill".

TABLE OF CONTENTS

Page

I. Title Page 1

II. Abstract 2

III. Acknowledgments 4

IV. Table of Contents 5

V. Text

Chapter I Introduction 6

Chapter II Materials Investigated 11

Chapter III Experimental Equipment and Testing Procedures 13

Chapter IV Experimental Results 18

Chapter V Conclusions 30

VI. Bibliography and References 38

VIII. Appendices

A. Biaxial Specimen Testing Apparatus 40

B. Biaxial Specimen Design, Casting and Machining 42

C. Mounting Biaxial Specimens in Instron Grips 50

D. Cleavage Test Fracture Energy Evaluation 52

E. Analysis of CTBN R-151 Particle Size 55

F. List of Tables 59

G. List of Figures 65

CHAPTER I

Introduction

The term crazing was first used to describe the small hairline cracks which occurred on the surface of ceramics and were falsely assumed to indicate the onset of material cracking. Crazing can be initiated by a combination of tensile stress and an aggressive material environment, with craze lines forming perpendicular to the tensile stress axis.

Crazing in plastics is thermally reversible, has little effect upon static strength, increases impact strength and is sensitive to the following composition factors:

1. Presence of plasticizers
2. Foreign particles of material
3. Low molecular weight molecules

Kambour (1) describes craze morphology as thin, plate-like partially void regions within a polymeric matrix containing stretched polymer molecules interconnected with normal polymer surrounding the craze. X-ray scattering studies indicate that craze voids consist of rather spheroidal shaped holes of approximately 200 Å diameter embedded in the glassy polymer matrix.

Modern thermosetting resins used for structural materials or composite matrices have limited usefulness because of low fracture toughness with consequent susceptibility to catastrophic failure.

Elastomer particles in glassy polymer matrix materials can increase fracture surface energy, γ, by as much as an order of magnitude over that of unmodified material (2,3) and produce stress whitening (4) and shear bands (5) in tensile test specimens.

By introduction of elastomeric particles into the glassy matrix Bucknall and Smith (4) found that a finely dispersed secondary phase of these particles became chemically bonded to the matrix material. Small concentrations of the elastomer caused increased crazing of the matrix material and an increase in matrix fracture energy. Crazing of the matrix generated significant visible stress whitening due to the fact that the craze behaves as an optically homogeneous medium and has a refractive index considerably lower than that of the normal polymer (1).

Sultan and McGarry (6), proposed that an elastomer having primary reactive sites could produce optimum toughening of a brittle epoxy matrix by dissolution in the uncured thermosetting resin, with subsequent precipitation as a particulate second phase during the polymerization of the resin. Elastomer reactive sites would then be available for formation of primary bonds between elastomer particles and the resin matrix.

Fracture energy of elastomer modified EPON 828 epoxy* material polymerized with Curing Agent D* was found to increase with increasing size and concentration of precipitated rubber

---

*mfg. by Shell Chemical Co., New York, N.Y.

particles at a single elastomer concentration. Particle sizes, ranging from 200-12,000 angstroms, were fairly independent of curing temperature and elastomer molecular weight for specimens incorporating acrylomitrile-butadiene (CTBN)** modifying particles. Variations of acrylomitrile in the CTBN elastomer molecule do tend to affect final particle sizes (6).

An exact understanding of the mechanism by which rubber particles promote increased fracture roughness with accompanying stress whitening has not been fully developed. A simple energy mechanism which considers particles as crack arrestors or energy sinks could account for only 10% of impact strength in impact styrene materials (7) and 13-18% for PMMA (8). Kambour (8) proposed that rubber particles are promoters of localized plastic flow in high stress intensity zones at the tip of a crack and that the fracture surface energy, γ, is the sum of three terms:

$$\gamma = \omega_h + \omega_p + \omega_e$$

where

ω_h = Work of hole formation against the free surface energy of the polymer.

ω_p = Plastic work of craze formation.

ω_e = Viscoelastic energy of craze extension.

The third term, ω_e, contains the large difference in surface energy between a γ calculated theoretically from

---

**Hycar Rubber, B. F. Goodrich Chemical Co., Cleveland, Ohio

Griffith criterion fracture mechanics and the γ found in actual fracture experiments.

Sultan and McGarry (6) discuss a detailed account of various aspects of brittle-elastic crack propagation considerations in rubber modified matrix materials.

Sternstein and Ongchin (9) investigated criteria for shear yielding and craze formation using specimens machined from cast solid cylinders of polymethyl methacrylate (PMMA). Specimens were subjected to combinations of biaxial stress ranging from uniaxial tension to equal biaxial tension. Experimental data yielded a series of craze yielding envelopes as functions of temperature and stress for PMMA crazing and a second series yielding curves similar to a Von Mises envelope; also a function of temperature and stress. Each yielding mode produced curves of distinctly different form with symmetry about the equal biaxial stress line. In the shear yielding study, the samples were internally pressurized and immediately subjected to a constant axial strain rate until the yield point was reached. In the crazing study the specimens were pressurized, brought to a given axial load level and held in this biaxial stress state for ten minutes at which time crazing began to appear.

It is the intention of this investigation to apply stress techniques used by Sternstein and Ongchin (9) in their study of PMMA thermoplastic to a biaxial stress study of brittle EPON 828 thermoset plastic modified with a dispersion of various elastomer particles. The percentage of acrylonitrile

in the CTBN shall constitute the primary variation in each of the series of samples to be investigated.

CHAPTER II

Materials Used in Experimental Investigations

Five thermosetting epoxy compositions were investigated under biaxial stress conditions as discussed in Appendix A. Variation of CTBN elastomer particle molecular weight and acrylonitrile composition constituted the only variation of material used in casting the five types of biaxial specimens.

All specimen castings used EPON 828 resin, an Epichlorhydrin/Bisphenol A product, with an approximate molecular weight of 450, which was polymerized with 5% by weight of Curing Agent D, the tri (2-ethyl hexanoic acid) salt of 2,4,6 tri (dimethyl aminomethyl) phenol (6).

All specimen types, modified by inclusion of an elastomer, contained 10% by weight of random copolymer of acrylomitrile and butadiene (CTBN) (10). All castings were cured at 120°C for two hours, slowly cooled to 50°C and then post cured at 130°C for two hours followed by slow cooling to room temperature.

Four different CTBN elastomer compositions were employed, in modifying the thermoset epoxy materials used in specimen casting procedures of Appendix B, possessing the following average molecular weight and acrylomitrile content:

Elastomer Symbol	$\overline{M}_\omega$	VCN (% Acrylonitrile)
CTBN R-146	3,000	>25.0
CTBN R-150*	5,300	17.7
CTBN R-151	4,700	18.2
CTBN R-151**	4,700	18.2

---

*Insufficient R-150 CTBN was available for a complete determination of fracture surface energy and biaxial stress curve.

**R-151N was thought to be identical to R-151 but gave differing results, to be shown later.

The carboxyl groups at each end of the CTBN molecule are considered to be reactive sites possessing the ability for the liquid elastomer to polymerize and crosslink with other rubber molecules to form particles and also to provide the primary bonds between elastomeric molecules and the epoxy resin; forming an adhesive bond between the rubbery second phase and the glassy matrix (6).

CHAPTER III

Experimental Equipment and Testing Procedure

A. Introduction

Experimental investigation procedures using four types of equipment were used and included:

1. Cleavage tests which determined fracture surface energy, γ, using an Instron Universal Testing Machine.
2. Biaxial stress applied to hollow cylindrical specimens by the apparatus shown in Figure (4), and discussed in Appendix A.
3. Optical microscopy of biaxial specimen surfaces using transmitted and reflected light of a Reichert microscope. Micrographs were recorded on Polaroid prints.
4. Electron Scanning Microscopy (ESM) of cleavage and biaxial specimen surface materials. Micrographs were recorded on Polaroid prints.

Experiments were conducted on five material compositions which included:

1. EPON 828 + 5% Curing Agent D
2. EPON 828 + 10% CTBN R-146 + 5% Curing Agent D
3. EPON 828 + 10% CTBN R-150 + 5% Curing Agent D
4. EPON 828 + 10% CTBN R-151 + 5% Curing Agent D
5. EPON 828 + 10% CTBN R-151N + 5% Curing Agent D

B. Cleavage Testing

Four flat plates of epoxy material, one for each of the above compositions, with the exception of CTBN R-150, were cast between smooth glass plates using the standard cure and post cure procedures outlined previously.

Cleavage specimens were machined from the smooth plate castings with geometries identical to those used by Broutman and McGarry (22) as shown in Figure (7).

Cantilever specimens were secured in an Instron and tested at a cross head rate of 0.02 inch per minute. Materials containing CTBN left a permanent record of the crack length in-that points of crack initiation and arrest were stress whitened whereas regions of rapid crack growth maintained the color of the bulk material. The unmodified specimens left no permanent record of crack propagation and required marking points of crack arrest with a felt tipped pen on the cantilever during the testing of the material.

A number of CTBN modified cantilever specimens were tested at a reduced cross head rate of 0.01 inch per minute to determine rate effects upon crack initiation and propogation. It was not possible to induce an initial rapid crack growth in these specimens as they stress whitened the entire length of the slotted region. To overcome this difficulty the crosshead rate was momentarily increased to 0.02 inch per minute to induce an initial rapidly propogating crack; then the crosshead rate was reduced to 0.01 inch per minute after which the specimen exhibited both rapid crack

growth and crack arrest. This behavior is attributed to an inability to machine a truly sharp crack tip in the cantilever specimen, however once a sharp crack is produced the material behaves in a manner similar to that experienced with higher crosshead velocities.

C. Biaxial Stress Testing

A series of approximately ten cylinders were cast and machined for each of the five material compositions. Processes and techniques for producing these biaxial specimens are outlined in Appendix B.

The Instron machine was calibrated prior to specimen testing each day. Specimens were measured with a micrometer and then mounted in the specially designed testing grips using the steps of Appendix C.

At least one cylinder was tested to yielding or fracture from each material series, using one of the following test procedures:

1. Instron tension only, at 0.005 inch per minute crosshead rate to a tensile force where the load vs. time, as plotted by the Instron chart, is of zero slope or the specimen fractures. This load together with specimen cross sectional area provides uniaxial tensile yield stress, σ_a.
2. Hydraulic pressure only, with no applied Instron tensile load. Pressure is increased slowly by adjusting the nitrogen storage bottle pressure

regulator, shown in Figure (4), until the specimen crazes, plastically yields or fails in fracture. This test yields the hoop stress, σ_h, at which crazing or yielding occurs.

3. A combination of Instron tension and hydraulic pressure which yields various combinations of σ_a and σ_h, defining the crazing and shear yielding envelopes.

In these tests hydraulic fluid is first applied slowly to a desired pressure and maintained; the Instron is then started and continues to load the specimen until the specimen fractures or the slope of load vs. time is zero. Each test required approximately 30 minutes of continuously increasing tensile loading.

D. Optical Microscopy

A Reichert optical microscope was used for examination of material surfaces using both reflected and transmitted light sources. Optical micrographs were recorded using a Polaroid camera.

E. Electron Scanning Microscopy (ESM)

Stress whitened sections of cantilever and biaxial specimen surfaces were carefully cut and mounted on aluminum ESM holders, evacuated for several hours, flashed with a gold coating and inserted into the vacuum chamber of a Japan Electron Optics Laboratory Co., Ltd. (JEOLCO), Type JSM

electron scanning microscope. Standard JEOLCO operating instructions were followed in recording micrographs.

All samples were carefully handled to avoid damage and contamination of surface area during mounting and scanning operations.

CHAPTER IV

Experimental Results

A. Introduction

A minimum of three cantilever test specimens were cast, machined and tested for each of four material compositions previously described: EPON 828 (unmodified), CTBN R-151, CTBN R-151N and CTBN R-146. CTBN R-150 was not cleavage tested since a limited available supply of the elastomer precluded a thorough investigation of both cantilever and biaxial stressed castings. It was decided that use of this CTBN R-150 elastomer in a series of biaxial specimens would prove of more interest than an exact determination of γ from cantilever tests.

Three complete series of biaxial specimens consisting of approximately ten specimens per series were cast, machined and tested and consisted of the following material: EPON 828 (unmodified), CTBN R-151N and CTBN R-146. These specimens were tested at room temperature (approximately 74°F) using procedure and equipment discussed previously.

The surface of biaxial specimen #12, a specimen of particular interest which will be discussed later, was investigated under the transmitted and reflected light of the Reichert microscope and a number of micrographs were recorded.

Finally, the ESM was used to scan the cleavage surfaces of CTBN R-146, CTBN R-151, CTBN R-151N and a specimen of CTBN R-151N cured at a reduced temperature of 74°C. A large

number of surface samples were carefully sliced from the CTBN R-151N biaxial specimen #12, mounted and scanned with the ESM.

B. Cleavage Specimen Tests

Values of surface energy, γ, are compiled in Table I from cantilever specimens fractured in the Instron. Test data was processed using the analysis techniques of Appendix D.

The inclusion of CTBN R-151N elastomer particles within the EPON 828 matrix increased the fracture surface energy of the modified material by nearly an order of magnitude over that of unmodified EPON 828 whereas CTBN R-146 elastomer inclusion effectively less than doubled fracture surface energy.

The three materials are ranked in order of decreasing fracture surface energy or fracture toughness:

CTBN R-151N

CTBN R-146

EPON 828 (unmodified)

C. Biaxial Specimen Tests

The results of the tests of biaxial specimens are tabulated in Tables II-V. This data was used together with Instron chart data of load vs. time to give the graphs of Axial Tensile Stress vs. Hoop Tensile Stress and Axial Tensile Stress vs. Relative Engineering Strain for the three biaxial specimen materials. These graphs are shown in Figures (8 - 13).

Biaxial testing of CTBN R-150 and CTBN R-151 specimens was accomplished, however, the data from these experiments was not sufficient to generate curves similar to those listed above.

All specimens loaded with both axial and hoop stress were first pressurized to the desired hoop stress with hydraulic fluid* which was then maintained constant as the Instron applied increasing amounts of axial stress.

During the application of increasing stress the buttery yellow colored CTBN R-151, CTBN R-151N and CTBN R-150 specimens became increasingly opaque and milky white in appearance throughout the gage length. Release of hydraulic pressure and tension stresses appeared to reduce this whitening effect but did not completely reverse it. EPON 828 and CTBN R-146 specimens exhibited no evidence of stress whitening.

The onset of obvious permanent stress whitening appeared in the center of the gage length for CTBN R-151, CTBN R-151N and CTBN R-150 and at stresses only slightly less than those existing when large plastic deformation of specimen material became obvious. This stress whitening was greatest in specimens where stress bias was highest, a result similar to that of Sternstein and Ongchin (9) in their studies of biaxial stressed PMMA. Stress bias, σ_b, is defined by,

$$\sigma_b = |\sigma_a - \sigma_h|$$

---

*Dow-Corning 550 Fluid (Silicon Oil)

where,

σ_a = axial tensile stress

σ_h = hoop tensile stress

Stresses defining the yield envelopes were taken from the curves in Figures (9,11 and 13) at the point where the slope of Uniaxial Tensile Stress vs. Relative Engineering Strain became zero, with σ_h constant for each of the curves. In those cases where zero slope was not achieved, the stresses existing at fracture failure of the specimen were used.

Resultant values for σ_a and σ_h were determined using stress formulas for an open ended cylinder (11, 12). The axial tensile stress, σ_a, is derived from the formula:

$$\sigma_a = \frac{F}{A}$$

where,

F = Instron tensile load

A = cross sectional area of gage material perpendicular to the tensile axis

The resultant values for hoop tensile stress, σ_a, in an open ended cylinder are derived from:

$$\sigma_h = \frac{Pr}{t}$$

where,

P = hydraulic fluid pressure

r = mean cylinder wall radius

t = cylinder wall thickness

Biaxial specimens tested to failure exhibited a fracture surface perpendicular to the Instron tensile axis when $\sigma_a > \sigma_h$

and parallel to this axis when $\sigma_h > \sigma_a$. Large amounts of stress whitening occurred along fracture surfaces of CTBN R-151, CTBN R-151N and CTBN R-150 specimens but whitening was not observed on EPON 828 (unmodified) and CTBN R-146 fracture surface material.

Figures (8) and (10) reveal that EPON 828 (unmodified) and CTBN R-146 biaxial specimens yield in shear, defining a yield envelope similar in form to that of the Von Mises Yield Criterion (11, 12), plotted on Figure (8) for comparison purposes using,

$$Y = \{\tfrac{1}{2}[(\sigma_a - \sigma_h)^2 + \sigma_a^2 + \sigma_h^2]\}^{\frac{1}{2}}$$

where,

Y = tensile yield stress

σ_a = axial tensile stress

σ_h = hoop tensile stress

The yield envelope for CTBN R-151N is significantly different, has a form similar to that of the "crazing yield" envelope for PMMA (9) and is indicative of a brittle material exhibiting tensile type failure.

The obvious differences in yielding envelopes of the three materials suggests that a shear yielding mechanism exists in EPON 828 (unmodified) and in CTBN R-146 material each exhibiting ductile material characteristics, with a differing yield mechanism occurring within the CTBN R-151N material.

Differences in strength and relative ductility of the three materials are shown in Figures (8 - 13). Note that Figure (10) has two curves drawn to fit the experimental date.

Tensile strength for each of the three materials is approximately:

1.	EPON 828 (unmodified)	10,700 lb/in^2
2.	CTBN R-146	9,000 lb/in^2
3.	CTBN R-151N	8,370 lb/in^2

The ductility of these materials can be judged on a relative basis, all specimen gage lengths and radii are identical, and are ranked in order of decreasing ductility:

CTBN R-146
EPON 828 (unmodified)
CTBN R-151N

Ductility will be discussed further in the chapter of conclusions.

D. Optical Micrographs

Biaxial specimen #12, consisting of EPON 828 modified with CTBN R-151N elastomer, was stressed exclusively with hydraulic pressure to fracture. Just prior to fracture this specimen plastically deformed with a noticeable bulge at gage mid-length. This plastically deformed region contained innumerable, long, thin, white striations oriented at a small angle to the cylindrical axis, near the outer surface of the plastically deformed region.

Examination of the specimen surface in an optical microscope using transmitted light at 138.6x revealed numerous small fissures which gave the surface material a general appearance of cold drawing as is shown in Figure (14). A transmission micrograph at 283.5x revealed small hairline fissures as shown in Figure (15), in which elastomer rubber particles are visible, appearing to bridge the fissure at various points. Figure (16) is a transmission micrograph at 562.5x showing that two and sometimes three small cracks emanate from a rubber particle at the material surface.

These micrographs show that the CTBN elastomer particles are involved in the fracture process mechanism and appear to promote furcation, a possible matrix toughening process.

Previous investigations of elastomer toughening were accomplished on cleavage surface materials where complete crack propagation had occurred, however, the unfractured surface material of biaxial specimen #12 contains a permanent record of crack-elastomer interaction prior to material fracture.

E. Electron Scanning Microscopy (ESM)

1. Cantilever Surfaces: Elastomer particle size and fracture surface characteristics of CTBN R-151, CTBN R-151N, CTBN R-151N cured at 74°C and CTBN R-146 cantilever specimens were recorded on ESM micrographs. The unfractured surface of biaxial specimen #12 was also studied.

The 100X micrograph of Figure (17) shows a region of CTBN R-151N cantilever fracture surface with fast crack propagation at the left; then a region of crack arrested slow crack propagation with noticable stress whitening followed by a region of fast crack propagation.

The obvious difference in material surface is seen in the 1,000X micrographs of Figure (18) which is a slow crack propagation and Figure (19) which is a fast crack propagation region. Note that the surface region of slow propagation has extreme porosity and whitening as compared to the flat non-porous quality of the fast crack region.

This difference in material behavior can be attributed to the rate of crack propagation in the following manner. In the region of fast crack propagation, application of stress is much too rapid to allow absorption of fracture surface energy by stretching of polymer material; consequently the material propagates a crack in a brittle fashion with little stretching of these polymer chains.

In the region of slow crack propagation a triaxial stress created at the crack tip of the cantilever specimen exerts its forces over a period of time sufficient to allow absorption of fracture energy through actual stretching of matrix molecules in a manner similar to that proposed by Berry (23, 24). The presence of the elastomer particle in the matrix creates a region of high stress intensity at its periphery fostering the stretching of molecules and actual tearing of material from the region of the particle. This mechanism would account for

absorption of surface energy and consequently the toughening of the plastic material.

Rapid crack propagation begins when cantilever energy exceeds the fracture surface energy absorption of the material.

2. Statistical Particle Density: Careful examination of Figures (18) and (19) reveals that the diameter of matrix holes in the slow crack region is larger than apparent particle sizes in the fast crack region. This behavior is again attributed to possible matrix stretching in the triaxial stresses at the crack tip in slow crack propagation.

To test this hypothesis, CTBN R-151N material from a slow crack region was annealed at 120°C for two hours; then mounted and scanned with the ESM to see if contraction of material around the porous holes occurs, releasing residual stress held in the material. The results of the annealing experiment can be seen in the 3,000X micrograph of Figure (20). Annealing has indeed reduced the sharp edges of the fracture surface and the hole size is greatly diminished with small round particles protruding from many of the crater like hole structures. Whether these protrusions are actually rubber particles or structural anomalies is not certain. It is apparent, however, that a large amount of surface stress has been released by the annealing process.

A simple statistical study of Figures (18) and (20) was performed in an attempt to determine whether the protrusions noted in the annealed specimen could in fact be rubber particles. The details of this calculation are outlined in

Appendix E. Results show that if rubber particles have the diameter of the holes in unannealed CTBN R-151 material, then these particles would consist of 80% EPON 828 material and 20% CTBN R-151. This is a highly unlikely occurrence in a chemical system functioning as a two-phase system.

Analysis of the annealed surface material shows that the actual mass density of CTBN R-151 is approximately equal to the density of the small protruding particles seen in the micrograph of Figure (20). This evidence strongly suggests that the CTBN R-151 material exists as nearly pure second phase particles of a mean diameter of 0.66 microns distributed throughout the EPON 828 matrix material. This evidence further strengthens the argument that the large round holes of Figure (18) are voids around rubber particles created by the plastic deformation of matrix material during slow crack propagation under the influence of a triaxial stress. Large amounts of fracture energy are absorbed in this distortion with consequent material toughening.

3. Biaxial Specimen #12: Several specimens of the plastically deformed region of biaxial specimen #12 outer surface material were scanned with the ESM. Figure (21) is a 300X micrograph of a portion of one of the long, thin, white striations lying at a small angle to an axis orthogonal to the cylindrical axis of the biaxial specimen. Note the presence of the black voids in the material and that the two long, very thin voids present in the highly stressed whitened

material appear to be distorted from resultant high shear stress in the material. This is more clearly seen in Figure (22).

The 1,000X micrograph of Figure (23) shows that elastomer particles are deformed in ellipsoidal fashion with the major axis of the particle site being perpendicular to the tensile hoop stress and approximately parallel to the stress whitened striation. Examination of several particles on the periphery of the whitened zone shows a pair of band like whitened lines emanating from the tip of each particle site and symmetrical about a line perpendicular to the axis of tensile hoop stress. These bands are shown more clearly in the 3,000X micrograph of Figure (24) as two pair of bands emanate from the central particle in the grouping of three particles. The tensile hoop stress axis is oriented horizontally in this micrograph.

The micrograph of Figure (25) shows the results of an attempt to clean the surface of a section of biaxial specimen #12 with acetone prior to electron scanning. Acetone was applied with a damp lens tissue by lightly wiping the surface twice and then evacuating it for several hours.

As can be seen from the micrograph, the acetone stress relieved the surface material and obliterated all specimen detail leaving the surface with a very spongy appearance.

4. CTBN R-146 Fracture Surface: A fracture surface of CTBN R-146 cleavage specimen material was scanned with the ESM. The micrograph of Figure (26) was recorded in the

region of slow crack propagation and exhibits little evidence of stress whitening and material deformation. The surface appears to be brittle, a conclusion supported by the low γ value of Table I.

Magnifications of 10,000X revealed the presence of very small CTBN R-146 particles (relative to CTBN R-151N particle size) with no evidence of any porous surface material.

CHAPTER V

Conclusions

A number of conclusions can be drawn from the data and observations recorded from experiments on elastomer modified EPON 828 materials.

A. Particle Size

Cleavage specimen tests confirm the experimental results of Sultan and McGarry (6) in that the unmodified EPON 828 which fractures with low surface energy, γ, can be fracture toughened by inclusions of secondary phase elastomer particles in the EPON 828 matrix. Also it is shown that a decrease in acrylonitrile content of the CTBN elastomer tends to increase the particle size and promote material toughening.

If the mean particle diameter of 0.66 microns derived from the measurement of protruding particles on annealed cantilever specimen surface of CTBN R-151 is a measurement of actual elastomer particle diameter, then the particle like shapes on fast crack propagation surfaces seen in Figure (18) may be composed of an elastomer particle of CTBN surrounded by a CTBN rich zone or phase of CTBN and EPON 828 which in turn is surrounded by a region rich in EPON 828 with some CTBN, all of which is embedded in the matrix of EPON 828.

B. Biaxial Testing Conclusions

Biaxial specimens of CTBN R-146 and EPON 828 (unmodified) yielded in a ductile manner exhibiting the shear yielding

criterion of Von Mises with no macroscopic evidence of stress whitening, crazing or void formation. Specimens of CTBN R-151N, consisting of large elastomer particles, did not generate a Von Mises type yield curve but rather the cusped curve of Figure (12). This cusped curve has a shape similar to the craze yielding curve for PMMA (9) and strongly suggests that the material fails in a tensile manner and is brittle.

These differences, together with the fact that CTBN R-151N samples exhibited significant whitening, void formation as seen in Figure (22) and significantly higher fracture surface energy, indicate that the CTBN R-151N particles promote this behavior through mechanisms dependent upon particle size. Therefore, it is concluded that a threshold of particle size exists above which the behavior exhibited by CTBN R-151N is promoted.

Elongation of CTBN R-151N elastomer particle sites in a direction perpendicular to the hoop tensile stress axis and the radiation of band structure from the particle site tip at a small angle to the major axis of the elongated particle is of great interest. This behavior indicates that large shear forces are being exerted upon the particle site. The existence of this high shearing force is further demonstrated in Figure (21) which shows that voids in the whitened material are severly distorted in the direction of flow of the whitened line, whereas voids not located within the whitened area tend to remain round and undistorted. This evidence discloses the existence of large plastic shear flow of material within the stress whitened material region.

C. Stress Relieved Fracture Surfaces

Stress relieving of CTBN R-151 cleavage surface material, Figure (20), shows a drastic reduction in the dimensions of surface holes after annealing. It is concluded that this porous structure does indeed consist primarily of holes possibly created by the triaxial stress exerted on the material at the tip of the cleavage specimen crack. This stress exerted on material in the region of slow crack growth is applied over a period of time sufficient to allow plastic distortion of polymer material around the elastomer particle site. This large deformation may be part of the mechanism by which a large amount of fracture energy is absorbed in a toughening of the elastomer modified material.

D. Elastomer-Matrix Interaction

In the EPON 828-CTBN matrix the difference in coefficient of expansion between the glassy phase of EPON 828 and the rubber particles can create tension in the rubber particles (5). The epoxy is then under a tangential compression; reducing the tensile stress produced by an external load and drastically altering the maximum shear stress at the particle matrix interface. A Mohr's circle representation of stresses for a uniaxial tension with no compressive stress is shown in Figure (27). By considering existence of a possible compressive stress of the elastomer-matrix interface, σ_2, it is seen that the Mohr's circle of Figure (28) now has tensile and compressive stresses with maximum shear stress,

$$\tau_{max} = \frac{\sigma_1 - \sigma_2}{2}$$

where,

σ_1 = maximum tensile stress

σ_2 = maximum tangential stress

Sultan and McGarry (6) predicted that with this compressive stress induced by the elastomer particle, the maximum shear stress has increased and shear yielding can occur before tensile failure; at small angles to an axis orthogonal to the tensile axis.

Evidence from ESM micrographs tends to support this prediction as can be seen in Figures (23) and (24) where the particle tips appear to radiate shear type bands at a small angle to the major axis of the elliptical particle.

E. Biaxial and Cleavage Surfaces

Experiments with both biaxial and cleavage surfaces have shown that a cleavage surface provides a record of material behavior after a crack has passed through the material and fracture is completed. Examination of the stressed surface of biaxial specimens provides a look at material which is in the process of yielding and fracture with a record of distortions, voids and whitening actually locked into the material; providing a permanent record of material reaction to stress forces.

Biaxially stressed specimens therefore provide a means for further investigation of elastomer modified thermoset material fracture toughening mechanisms.

F. Ductility and Fracture Surface Energy

Fracture toughness values from Table I together with the curves of Figures (8 - 13) indicate that inclusion of large elastomer particles in CTBN R-151N material greatly increases EPON 828 fracture toughness but reduces the strength and ductility of the material. The CTBN R-151N tensile type yielding envelope suggests that the material is failing in a brittle manner. Unmodified EPON 828 and EPON 828 modified with CTBN R-146 elastomer (small particles) display greatly reduced fracture toughness relative to CTBN R-151N material. However, these materials exhibit shear type yielding together with large plastic distortions during biaxial testing and are more ductile than is the CTBN R-151N material.

It is concluded that large particles enhance fracture toughness of the matrix but that their presence has a deleterious effect upon material ductility. Small particles of CTBN R-146 seem to enhance ductility and fracture toughness with little diminution of material strength relative to unmodified EPON 828.

G. Topics for Further Study

Much of the experimental work accomplished in this thesis has created a large number of questions in addition to furnishing a few answers regarding the behavior of elastomer particles in stressed EPON 828 matrix material.

Further investigations are recommended, some of which include:

1. Additional testing of a single composition, large particle, set of biaxial specimens at a variety of temperatures is needed to determine the curves of axial tensile stress vs. hoop tensile stress as a function of temperature. Changes in the form of these curves may indicate that a temperature exists below which elastomer particle toughening mechanisms will not function. A study of such specimens may produce information on particle morphology influences upon fracture toughening.

2. Biaxial specimens composed of variations of the modifying CTBN elastomer should be tested to determine the threshold of particle size and character above which yielding behavior similar to that of CTBN R-151N is observed. If this is determined, it may be possible to correlate particle size with the stress whitening and toughening of the material by noting differences in microscopic material behavior.

3. A large amount of further investigation remains in determining the nature of the bands which emanate from elastomer particle sites, distorted in stressed biaxial specimen surface material.

4. Further study of the elastomer particle sites is needed in both biaxial and cleavage specimens. A knowledge of elastomer-matrix bonding is desired in-order-that the magnitude of stress concentrations can be determined which in turn may aid in revealing the mechanism of void formation and stress whitening of the modified epoxy material.

5. Further investigation of the large holes found in CTBN R-151 cleavage surface material in slow crack propagation regions is desirable. It remains to be determined experimentally and theoretically that these holes result in matrix toughening through the large energies absorbed in plastically deforming the material surrounding them.

6. A study of the shear band experiments done by Ludwig (26) on CTBN modified EPON 828 material should be accomplished with the objective of possibly applying the results of this work to the observation of small bands emanating from elastomer particle sites in stress whitened biaxial specimen materials.

7. Explanation of reasons for the observed occurence of small voids throughout the stress whitened regions of biaxial specimen materials has been covered only superficially and requires further study.

8. Biaxial specimen surface material which has been stressed to whitening should be annealed and scanned with ESM to see if the distortion of particle sites within the material has been relaxed and if the particles are once again circular in shape.

9. The entire question of which mechanism forms crazing and which mechanism promotes shear banding must be reviewed and the relationship of stress whitening and particle deformation to material toughening must be determined.

10. Further investigation is necessary to determine the relationship of elastomer particle size to fracture toughness and to ductility. It now appears that large particles promote large amounts of stress whitening and increased fracture surface energy but at the same time they reduce the ductility of the material. Small particles do not create stress whitening but seem to promote ductility even though they toughen an EPON 828 matrix to a much lesser extent than do CTBN R-151N elastomer particles.

It is realized that an even larger listing of topics requiring further study could be compounded for these elastomer modified materials but those listed above are a few of the more interesting questions which must be investigated for these materials.

REFERENCES

1. Kambour, R.P., "Stress-Strain Behavior of the Craze", Polymer Engineering and Science, Vol. 8, No. 4, October 1968.

2. McGarry, F.J., Willner, A.M. and Sultan, J.N., "Effects of Interstitial Inclusions in Fiber Reinforced Composites", M.I.T. Technical Report AFML-TR-69-86, May 1969.

3. McGarry, F.J., Willner, A.M. and Sultan, J.N., "Relationships Between Resin Fracture and Composite Properties", M.I.T. Technical Report AFML-TR-67-381, December 1967.

4. Bucknall, C.B. and Smith, R.R., "Stress-Whitening in High Impact Polystyrene", Polymer, 6, 1965.

5. Andrews, R.D.,Jr., Allison, S.W., Ender, D.H., Kimmel, R.M., and Whitney, W., "Research Study on Cold Drawing Phenomena in High Polymers", M.I.T. School of Engineering, Technical Report 67-10-CM, Chapter IV, August 1966.

6. Sultan, Jacques N. and McGarry, Frederick J., "Microstructural Characteristics of Toughened Thermoset Polymers", M.I.T. School of Engineering, Research Report R69-59, October 1969.

7. Newman, S. and Strella, S., J. Appl. Poly. Sci, 9, 2297, 1965.

8. Kambour, Roger P., Applied Polymer Symposia, No. 7, 215, edited by Henno Keskkula, Interscience Publishers, New York City, 1968.

9. Sternstein, S.S. and Ongchin, L., "Yield Criteria for Plastic Deformation of Glassy High Polymers in General Stress Fields", Polymer Preprints, Vol. 10, No. 2, pp. 1117-1124, September 1969.

10. Drake, R.S. and MC Carthy, W.J., "Liquid Butadiene/Acrylonitrile Polymers with Reactive Terminals", Rubber World, pp. 51-56, October 1968.

11. Timoshenko, S. and Young, D.H., Elements of Strength of Materials, D. Van Nostrand Company, Inc., 5th Edition, pp. 294-313, 1968.

12. Crandall, Stephen H. and Dahl, Norman C., An Introduction to the Mechanics of Solids, McGraw-Hill Book Company, Inc., Chapter IV, 1959.

13. Davis, E.A. and Parker, E.R., J. Appl. Mech., Vol. 15, p. 201, 1948.

14. Davis, E.A., *J. Appl. Mech.*, Vol. 12, p. 13, 1945.

15. Davis, E.A., *J. Appl. Mech.*, Vol. 15, p. 216, 1948.

16. Bridgeman, P.W., *The Physics of High Pressure,* New York, 1931.

17. Bridgeman, P.W., *Studies in Large Flow and Fracture*, New York, 1952.

18. Taylor, G.I. and Quinney, H., *Trans. Roy. Soc. (London)*, A-230, 323 (1931)

19. Bowden, P.B. and Jukes, J.A., *J. Mat. Sci., 3*, 183, (1968).

20. Zaslawsky, M., "The Effect of Biaxial Stress on the Creep Properties of Polymethyl Methacrylate", *Polymer Engineering and Science*, Vol. 9, No. 2, pp. 105-108, March 1969.

21. Sternstein, S., Ongchin, L. and Silverman, A., *Applied Polymer Symposia*, Vol. 7, Interscience Publishers, New York City, 1968.

22. Broutman, L.J. and McGarry, F.J., "Fracture Surface Work Measurements on Glassy Polymers by a Cleavage Technique", *J. Appl. Polymers Sci.*, 9, pp. 589-608, (1965).

23. Berry, J.P., *J. Polymer Sci.*, A1, 933, (1963).

24. Berry, J.P., *J. Polymer Sci., 50*, 107 and 313, (1961).

25. Sultan, Jacques N., Personal communication.

26. Ludwig, Carl L., Personal communication.

APPENDIX A

Biaxial Specimen Testing Apparatus

A. Design and Construction of Instron Grips

An Instron testing machine grip assembly was designed and constructed and is shown in Figure (1). Components of the assembly include an upper grip, lower grip, stainless steel plunger, three high pressure o-rings and a plexiglass shield.

The lower grip and plunger shown in Figure (2) contain threads for securing a biaxial specimen to the grip, a threaded receptacle for attaching the steel plunger, threaded receptacle for connection of high pressure hydraulic hose and a channel for directing hydraulic fluid to the center of a biaxial specimen.

An upper grip shown in Figure (3) contains threads for biaxial specimen attachment, a lower relief port with screw plug for purging air as hydraulic fluid fills the specimen and an upper relief port bleed-off for hydraulic fluid leakage past the plunger o-ring during testing. The plunger head is fitted with a 1,500 psi o-ring which fits between the two relief ports in the 1.25 inch channel when the grip assembly is completed.

The steel plunger transmits all axial hydraulic force into the bottom grip and causes the cylindrical specimen to act as an open ended cylinder during testing.

A 3.65 inch long plexiglass sleeve fits between the two grips and rests on a narrow seat cut into the circumference of the lower grip creating a safety shield and hydraulic fluid reservoir in the event of biaxial specimen fracture.

A complete assembly mounted in the Instron is shown in Figure (4).

B. Hydraulic Fluid Pressurizing Equipment

Hydraulic fluid pressurizing components are shown in Figure (4) and consist of the following equipment:

1. Nitrogen compressed gas cylinder and regulator valve
2. One gallon capacity hydraulic accumulator unit, Greer-Olaer Model 30A-1B
3. One hydraulic gauge of 2,000 psi capacity
4. High pressure tubing, pipe connections and regulating valves
5. Dow-Corning 550 fluid (silicon oil)

Nitrogen gas is introduced into the bottom of the accumulator vessel inflating a rubber membrane which forces the hydraulic fluid out the top of the accumulator, through a valve and hose to the lower Instron grip.

Hydraulic pressure is controlled by adjustment of the compressed nitrogen bottle air regulator valve. The pressurizing equipment listed above was successfully statically tested at 1,450 psi for one hour prior to use in biaxial testing experiments.

APPENDIX B

Biaxial Specimen Design, Casting and Machining

A. Specimen Geometrical Design

Geometry of the biaxially stressed specimen consists of a thin walled cylinder, shown on the right in Figure (5), with carefully machined threads at either end for securing it to Instron grips. The biaxial specimen must withstand the tangential hoop stress induced by internal pressure and Instron tensile stress applied parallel to the cylinder axis.

As discussed in References (9, 11, 12, 13, 14, 15, 16, 17, 18, 19, 20 and 21), specimen geometry is a compromise of various design factors. A radial stress gradient is produced by internal hydraulic pressure, creating higher stress on inner wall areas than the ambient pressure stress on the outer wall. This radial stress gradient, σ_3, was minimized by achieving a small ratio of wall thickness to mean specimen diameter. The tangential or hoop stress also varies from the inner to outer surface and its variation is again minimized by a small thickness to mean diameter ratio. These desirable design factors are countered by a requirement to minimize material shrinkage stresses created during casting and curing of specimens and maintaining experimentally applied stresses within the capacity of the pressure system and tensile tester. Minimum specimen thickness to diameter ratio is further restricted by the ability to produce accurately machined specimens.

An estimate of maximum tensile and hydraulic forces necessary for testing specimens of this geometry was obtained using epoxy-CTBN ultimate tensile strength of 10.67×10^3 lb/in^2 (2) and considering the specimen to be an open ended cylinder.

Maximum anticipated Instron tensile force was estimated to be,

$$F_{axial} = 2{,}747 \text{ lb}$$

and maximum anticipated hydraulic pressure was estimated at,

$$P_{hyd.} = 1{,}015 \text{ psi}$$

These test forces were considered obtainable with specimen geometry of Figure (6); subsequent design was based on these forces.

A numerical check of the tangential stress variation from the inner to the outer wall of the specimen indicates a variation of 4.75% from mean tangential stress.

Radial stress, σ_3, is considered to be negligible according to Crandall and Dahl (12) in that,

$$\frac{t}{r} << 1$$

B. Design of Specimen Molds

Two pieces of stainless steel pipe and an aluminum spacer are used to form the sample mold. The inner mold pipe or barrel has a highly polished surface with outside diameter of 1.250 inches and a length of 6.50 inches. The outer mold

pipe or sleeve is unpolished with inside diameter of 2.00 inches and a length of 6.00 inches. The aluminum spacer is cut to give a snug fit with the barrel and sleeve and to space them concentrically, forming a 0.375 inch casting wall thickness as shown at the left in Figure (5).

This mold design is considered highly desirable and removes the requirement to drill, ream and polish the inner surface of specimens made from solid castings of epoxy material.

C. Casting of Biaxial Specimen Cylinders

Two basic specimen material types were cast for biaxial testing, the first consisted of EPON 828 and Curing Agent D with the second consisting of EPON 828, various CTBN's and Curing Agent D. Great difficulty was encountered in obtaining perfectly smooth barrel surfaces on cast specimens. Approximately 80% of the castings contained hemispherical indentations or axial troughs which were not caused by entrapped air but were finally attributed to surface tension phenomena.

An attempt to salvage the 80% unsatisfactory specimens entailed reaming of the inner surface to a depth which removed all imperfections; followed by polishing of the reamed surface. This process was found to be unsatisfactory for three reasons:

1. The reaming tool created "skid" marks on the surface as it was rotated through the specimen.
2. Subsequent sanding and polishing of the reamed surface was difficult and unsatisfactory in that it failed to

remove "skid" marks without giving a variable diameter over the length of the specimens' inner surface.

3. Measurement of the inside diameter of specimens is difficult to obtain accurately and is impossible if sanding and polishing render the surface non-circular.

It is considered imperative that the inside specimen geometry should be formed by the barrel of the mold, in-that mechanical formation of this surface is unsatisfactory.

A lengthy investigation of casting parameters and procedures revealed a satisfactory method for casting perfectly smooth barrel surfaces with production of approximately 100% success. This casting procedure differs slightly dependent upon whether CTBN is present or absent.

Casting procedure for EPON 828, 10% CTBN and 5% Curing Agent D consists of the following sequence:

1. Lightly polish the mold barrel with 000 grade steel wool. To do this wrap the steel wool around the mold and rotate the mold within the steel wool; slowly work the mold through the steel wool axially as the barrel is continually rotated. Press the steel wool to the barrel only lightly.
2. Wipe the barrel with a dry, clean, soft cloth to remove dust, steel wool and old FreKote 33* particles.

---

*Mold release agent mfg. by FreKote, Inc., Indianapolis, Ohio

Do not touch the barrel with oily hands; gloves are recommended.

3. Spray the barrel surface with a light coat of FreKote 33 release agent.
4. Place the barrel into an oven at 60°C for approximately 10 minutes.
5. Take the barrel from the oven and allow it to cool for approximately 10 minutes, then spray lightly with another coating of FreKote.
6. Remove old FreKote particles from the inner surface of the sleeve as any particles may become incorporated in the casting and will cause axial fractures in the material.
7. Spray the aluminum spacing ring and inner sleeve surfaces with a coating of FreKote.
8. Assemble the three mold components and place the assembly into the oven at 60°C for at least 15 minutes.
9. Measure the desired amount of EPON 828 on a balance in a clean, dry beaker.
10. Add the desired amount of CTBN to the EPON beaker.
11. Place the beaker in a mineral oil bath at 275°F insuring that the bath liquid level is above that of the EPON-CTBN level in the beaker.
12. Wrap a steel spatula with several turns of the clean, dry, white cloth which has no dangling strings or lint. Secure this wrapping with a fine string.

Coarse string and wooden spatulas will release entrapped air which is unsatisfactory.

13. Stir the EPON-CTBN mixture with this cloth wrapped spatula as they are heated in the oil bath. Air will escape the cloth as the mixture permeates it, but air bubbles will collapse on the surface when the CTBN-EPON mixture approaches bath temperature.
14. Leave the EPON-CTBN mixture in the bath until the solution is fully transparent and all surface and subsurface bubbles and froth have disappeared. This often takes 20-30 minutes.
15. When the EPON-CTBN mixture is clear and hot, degas the solution in a vacuum desiccator for 15 minutes. The solution must be hot for positive results.
16. Place the beaker back in the oil bath and heat until no bubbles exist or until the solution is at 250°F. If bubbles persist, continue degasing. Always reheat the solution after degasing.
17. Remove the beaker from the oil bath and place on the balance. Allow the solution to cool with occasional stirring until a thermometer reads 100°C.
18. Remove the mold from the oven and place on a table ready for pouring of the epoxy.
19. Add the desired amount of Curing Agent D to the EPON-CTBN solution and stir thoroughly until the solution is entirely homogeneous.

20. Pour the epoxy solution into the mold taking care to keep the spatula wrapping below the surface of the solution in the beaker.

21. Prior to complete filling of the mold take the spatula and lightly brush the wrapping up and down the sides of the barrel. Do not press heavily as this will remove FreKote and the hardened epoxy will stick to the barrel.

22. Fill the mold to the top and let it sit for 10-15 minutes on the table.

23. Place the mold in the oven and cure at 120°C for two hours, after which the sample is allowed to cool to 50°C and is then post cured at 130°C for two hours and finally allowed to cool to room temperature in the oven.

To cast EPON 828 - Curing Agent D samples the only alteration of the above procedural steps is to reduce the temperature in step 17 to 80°C when pouring the solution into the mold.

D. Removal of Biaxial Specimen From Mold

Biaxial specimen castings are most easily removed from the mold after post curing, at a temperature of 40°C using an arbor press.

E. Machining of Biaxial Castings

After removal from its mold the casting is pressed onto a 1.250 inch mandrel and mounted in a turning lathe. It is

extremely important that an indicator be used for lathe alignment prior to accomplishment of a machining process on the specimen, insuring uniform specimen thicknesses. The casting is then turned to 1.875 inches outside diameter and the ends are squared off to give the 5.375 inch cylinder length shown on the left in Figure (5).

The cylinder is again mounted on the mandrel and one inch grip thread lengths are marked at either end. A round cutting head of 1 1/2 inch diameter is used to cut the gage region of the specimen using a final pass, cut depth of less than 0.005 inch. The diameter of the center of the gage length is further reduced 0.010 inch by tapering the cut from no cut at the ends to 0.010 inch at the center. This is done to induce yielding at the center of the gage length. Central gage diameter is now approximately 1.365 inches.

The biaxial specimen is then polished with the finest grade paper available and is in a form similar to that of the center specimen in Figure (5).

Final machining consists of threading both ends of the specimen with 10 threads per inch of 0.075 inch depth. A completely machined specimen is shown on the right in Figure (5) and is now ready for testing.

APPENDIX C

Mounting Biaxial Specimens in Instron Grips

Biaxial specimens must be placed in the grips with great care to insure a successful test. The following stepwise procedure is required:

1. Place the lower grip in the receptacle of the moving beam of the Instron and secure it with a pin.
2. Insure that a 2.004 inch O.D., 1,500 psi O-ring is clean and lying flat in the bottom of the biaxial specimen receptacle.
3. Screw the biaxial specimen into the lower grip and tighten hand tight.
4. Screw the steel plunger into the threaded receptacle in the lower Instron grip; when tight, back off two complete turns. Insure that the 1.255 inch O.D., 1,500 psi O-ring on the plunger head is clean and undamaged.
5. Place the plexiglas shield over the sample and seat it firmly upon the machined shoulder of the lower grip.
6. Carefully place a 2.004 inch O.D., 1,500 psi O-ring on top of the biaxial specimen, centering the O-ring to avoid jamming damage from the threads of the upper grip.
7. Screw on the upper Instron grip hand tight and secure it to the load cell receptacle of the Instron.

8. To fill the specimen with hydraulic fluid merely apply a low nitrogen pressure to the accumulator (50 psi or less) and slightly open the hydraulic fluid outlet value on top of the accumulator. It is not necessary to remove the screw in the air bleed-off port to fill the specimen as air will pass by the plunger O-ring but hydraulic fluid will not leak by.

9. Biaxial testing is now ready to commence.

It is imperative that step 4 above, be followed exactly as any misplacement of the plunger may position the O-ring near a bleed-off port. High pressures will cause the O-ring to be pushed into the port and a piece will shear off, rendering the O-ring useless.

APPENDIX D

Cleavage Test Fracture Energy Evaluation

Fracture energy values of four epoxy materials were determined using the cleavage technique described by Broutman and McGarry (22). Instron tensile force was applied, at a rate of 0.02 inch per minute, to the drilled holes at the end of the specimen shown in Figure (7). A mechanically initiated crack then propagates along the central slot material with the specimen behaving as a centilever with fixity at the unsplit end.

Fracture surface work is given by γ as,

$$\gamma = \frac{n}{4} \frac{F\delta}{\omega L}$$

where,

F = Applied force

δ = Deflection of one cantilever

ω = Crack width

L = Crack length

n = An experimental constant

The instron records load vs. time as the specimen is cleaved. Crack length is measured directly during the test or upon test completion by measuring the distance between whitened spots on the slot material. These whitened spots occur only for material which contains CTBN R-151 and CTBN R-151N. Crack progress on other specimens must be marked with a felt tipped pen during testing.

The constant, n, is the slope of a plot of log (F/δ) vs. log (L) since,

$$F = \frac{a\delta}{L^n}$$

for a cantilever, where "a" is a constant.

Most cleavage samples will exhibit several successive rapid crack propagations as the sample is tested to failure, allowing several determinations of γ from a single cantilever specimen. The γ value of the initial and final rapid propagation is often significantly different from the average; this may be due to imperfect machining of the notch at the initiating end of the specimen or a loss of cantilever fixity at the end where final propagation occurs.

Final calculations of fracture surface energy in this investigation used the following expression for γ,

$$\gamma = \frac{A_I * \frac{V_I}{V_c} * S * K * n}{2\ \ell\ \omega}$$

where,

γ = Fracture surface energy (erg/cm^2)

A_I= Integrator area (in-lb)

V_I= Instron crosshead velocity (in/min)

V_c= Instron chart velocity (in/min)

S = Instron load scale (lb full scale)

ℓ = Crack length (cm)

ω = Crack width (cm)

$K = 11.31 \times 10^5$ ergs/in-lb

n = Experimental constant

Values for n were determined as outlined previously.

APPENDIX E

Analysis of CTBN R-151 Particle Size

Annealed and unannealed cleavage surface specimens of CTBN R-151 were scanned with the ESM as shown in Figures (20) and (18) respectively. The large reduction of fracture surface hole diameter in the annealed specimen, with resultant protrusion of small particle masses, suggests that the surface has stress relieved, leaving rubber particles exposed.

By calculating the density of CTBN R-151 present in a unit volume of the modified matrix and comparing this to the volumes of the voids in Figure (18) and small particles in Figure (20) it was found that the small particles of the latter have a material volume sufficient to accommodate the volume which would be occupied by pure second phase particles of CTBN R-151.

The calculations were accomplished in the following manner. A square of 2 cm on a side was cut from cardboard and placed on Figure (18). The number of holes within the square were then counted. This was done at random locations over the surface and an average particle density of 4.16 particles per cm^2 was derived. This gives an actual surface particle density of,

$$\rho_p = 4.16 \times 10^6 \text{ particles per cm}^2.$$

Next an average particle diameter of 0.2 cm was measured, giving a particle volume of,

$$V_p = \frac{4}{3}\pi(2 \times 10^{-4})^3 = 33.5 \times 10^{-12} \text{ cm}^3$$

It is assumed that any plane fracture surface area will display holes for a particle if the fracture plane passes through any portion of the particle, i.e., at the very top, bottom or equator. Thus, the fracture surface represents a statistical distribution of particles within a specimen cross section one particle diameter in depth. One cubic centimeter of specimen will contain n_ℓ statistical particle layers,

$$n_\ell = \frac{1}{D_m}$$

where,

n_ℓ = number of particle layers per centimeter of depth

D_m = mean particle diameter

For the material of Figure (18) there are $n_\ell = 5{,}000$ particle layers per centimeter of depth and the total number of particle holes per cubic centimeter of material, N_T, is,

$$N_T = n_\ell * \rho_P = 20.8 \times 10^9 \text{ particles/cm}^3$$

Total particle volume, V_T, is found to be $V_T = N_T V_P = 0.696 \text{ cm}^3$ of particles in each cubic centimeter of specimen.

The number of grams of CTBN R-151 necessary to fill this particle volume, V_T, is found to be,

$$\omega_e = 0.92\ V_T = 0.64 \text{ gm}$$

where,

ω_e = grams of CTBN in each cubic centimeter of modified material

0.92 = specific gravity of CTBN R-151

Actual mass of CTBN R-151 in the specimen material can be derived from the original composition of the material using the densities of EPON 828 and CTBN R-151 which were supplied by Sultan (25):

EPON 828 = 1.22 g/cm^3

CTBN R-151 = 0.92 g/cm^3

Therefore an EPON 828 and 10% CTBN R-151 composition contains 0.1075 gm CTBN R-151 in each cubic centimeter of material.

Comparison of true and calculated masses of CTBN R-151 in the specimen material reveals that five times more elastomer is needed to fill the holes of the size shown in Figure (18) than actually exists or alternately, the particles would have to consist of approximately 80% EPON 828 and 20% CTBN R-151 to give the particle volumes indicated. The latter conclusion is not considered feasible in that a well defined second phase would not seem likely for particles containing such great quantities of EPON 828.

A similar analysis of the volume of the small protruding particles of Figure (20) was conducted. A mean particle diameter, D_m', was used:

$$D_m' = 0.66 \times 10^{-4} \text{ cm}$$

This mean particle diameter yields,

$$n'_\ell = 1.5 \times 10^4 \text{ layers/cm}$$

and a particle volume of,

$$V'_P = 1.23 \times 10^{-12} \text{ cm}^3/\text{particle}$$

A micrograph survey yielded a density of surface particles of,

$$\rho'_P = 5.75 \times 10^6 \text{ particles/cm}^2$$

Therefore,

$$N'_T = 86.2 \times 10^9 \text{ particles/cm}^3$$

and,

$$V'_T = 10.6 \times 10^{-2} \text{ cm}^3 \text{ of particles/cm}^3 \text{ of specimen}$$

The mass of CTBN R-151 required to fill the protruding particles of this micrograph is found to be,

$$\omega'_e = 0.097 \text{ gms}$$

As noted in the above analysis by considering the protruding particles to be a relatively pure second phase of CTBN R-151, the volume of these particles closely matches the volume density of the CTBN R-151 actually present. It is concluded that the large holes of Figure (18) are caused by plastic stresses during slow cleavage of the material and that they are not rubber particles.

APPENDIX F

List of Tables

Table — Page

I Fracture Surface Energy of CTBN Modified EPON 828 Cured with Curing Agent D 60

II Biaxial Specimen Yield Stress of Unmodified EPON 828 61

III Biaxial Specimen Yield Stress of CTBN R-146 Modified EPON 828 62

IV Biaxial Specimen Yield Stress of CTBN R-151 Modified EPON 828 63

V Biaxial Specimen Yield Stress of CTBN R-151N Modified EPON 828 64

TABLE I

Fracture Surface Energy of CTBN

Modified EPON 828 Cured* with Curing Agent D

Type CTBN	CTBN Conc. (PPh)	Fracture Surface Energy (10^5 erg/cm^2)
R-146	10.0	3.32
R-151**	10.0	7.67
R-151N	10.0	15.48
EPON 828 (unmodified)	10.0	1.75

---

*Cured at 120°C for two hours.

**2pph Curing Agent D, all others 5pph Curing Agent D. This was done by accident and is included for general information only.

TABLE II

Biaxial Specimen* Yield Stress of Unmodified EPON 828

Sample Number	Tensile Stress (ksi)	Hoop Stress (ksi)
13	0.00	8.89
16	10.83	0.00
23	12.94	6.02
24	10.40	8.90
25	11.85	7.63
26	9.79	0.00
27	10.00	10.39
28	10.00	2.25
33	10.67	2.72
49	9.10	8.13
50	8.24	9.06
51	8.75	8.82

---

*All specimens unreamed.

TABLE III

Biaxial Specimen* Yield Stress of CTBN R-146

Modified EPON 828

Sample Number	Tensile Stress (ksi)	Hoop Stress (ksi)
38	9.00	0.00
39	0.00	8.86
40	8.89	1.75
41	9.24	2.97
42	8.92	4.23
43	8.54	5.83
44	0.00	9.57
45	7.72	7.42
46	2.26	8.49
47	6.42	8.03

---

*All specimens unreamed.

TABLE IV

Biaxial Specimen Yield Stress of CTBN R-151

Modified EPON 828

Sample Number	Reamed (R) or Unreamed (U)	Tensile Stress (ksi)	Hoop Stress (ksi)
2	U	0.00	9.25
3	U	7.27	4.32
4	U	7.10	3.75
6	U	7.87	2.64
7	U	8.34	4.93
8	U	7.48	8.80
9	R	7.24	7.65

TABLE V

Biaxial Specimen Yield Stress of CTBN R-151N Modified Epon 828

Sample Number	Reamed (R) or Unreamed (U)	Tensile Stress (ksi)	Hoop Stress (ksi)
11	R	7.67	0.00
12	U	0.00	7.75
18	R	6.03	7.42
19	R	8.09	6.41
20	R	8.13	5.38
21	U	8.30	0.00
22	R	7.83	2.30
29	U	8.16	3.56
30	U	8.40	1.78
31	U	5.67	8.02
32	U	1.79	7.87
48	U	7.92	6.65

APPENDIX G

List of Figures

Figure Page

1 Instron Grip Assembly Used in Biaxial Testing 67

2 Instron Lower Grip Cross Section 68

3 Instron Upper Grip Cross Section 69

4 Biaxial Testing Apparatus 70

5 Biaxial Specimen Machining Sequence 71

6 Biaxial Specimen Cross Section 72

7 Cleavage Specimen 73

8 Biaxial Specimen Axial Tensile Stress, σ_a, vs. Hoop Tensile Stress, σ_h, for EPON 828 Modified with CTBN R-146 (Small Particles) 74

9 Biaxial Specimen Axial Tensile Stress, σ_a, vs. Relative Engineering Strain for EPON 828 Modified with CTBN R-146 (Small Particles) 75

10 Biaxial Specimen Axial Tensile Stress, σ_a, vs. Hoop Tensile Stress, σ_h, for Unmodified EPON 828 76

11 Biaxial Specimen Axial Tensile Stress, σ_a, vs. Relative Engineering Strain for Unmodified EPON 828 77

12 Biaxial Specimen Axial Tensile Stress, σ_a, vs. Hoop Tensile Stress, σ_h, for EPON 828 Modified with CTBN R-151N (Large Particles) 78

13 Biaxial Specimen Axial Tensile Stress, σ_a, vs. Relative Engineering Strain for EPON 828 Modified with CTBN R-151N (Large Particles) 79

14 Optical Micrograph of CTBN R-151N Biaxial Specimen Surface in Reflected Polarized Light (138.6x) 80

Figure Page

15 Optical Micrograph of CTBN R-151N Biaxial Specimen Surface in Transmitted Polarized Light (283.5x) 80

16 Optical Micrograph of CTBN R-151N Biaxial Specimen Surface in Transmitted Polarized Light (562.5x) 80

17 Cantilever Cleavage Surface of CTBN R-151N Cured at 74°C 81

18 Cantilever Cleavage Surface, Slow Crack Propagation in CTBN R-151 81

19 Cantilever Cleavage Surface of CTBN R-151N, Fast Crack Propagation 82

20 Annealed Cantilever Cleavage Surface of CTBN R-151, Slow Crack Propagation 82

21 Biaxial Specimen Surface, CTBN R-151N 83

22 Biaxial Specimen Surface, CTBN R-151N 83

23 Biaxial Specimen Surface, CTBN R-151N 84

24 Biaxial Specimen Surface, CTBN R-151N 84

25 Acetone Wiped Surface of CTBN R-151 85

26 Cantilever Cleavage Surface of CTBN R-146, Slow Crack Propagation 85

27 Mohr Circle for Specimen in Uniaxial Tensile Stress 86

28 Modified Mohr Circle in the Vicinity of a Rubber Particle for the Case where σ_2 is Negative 86

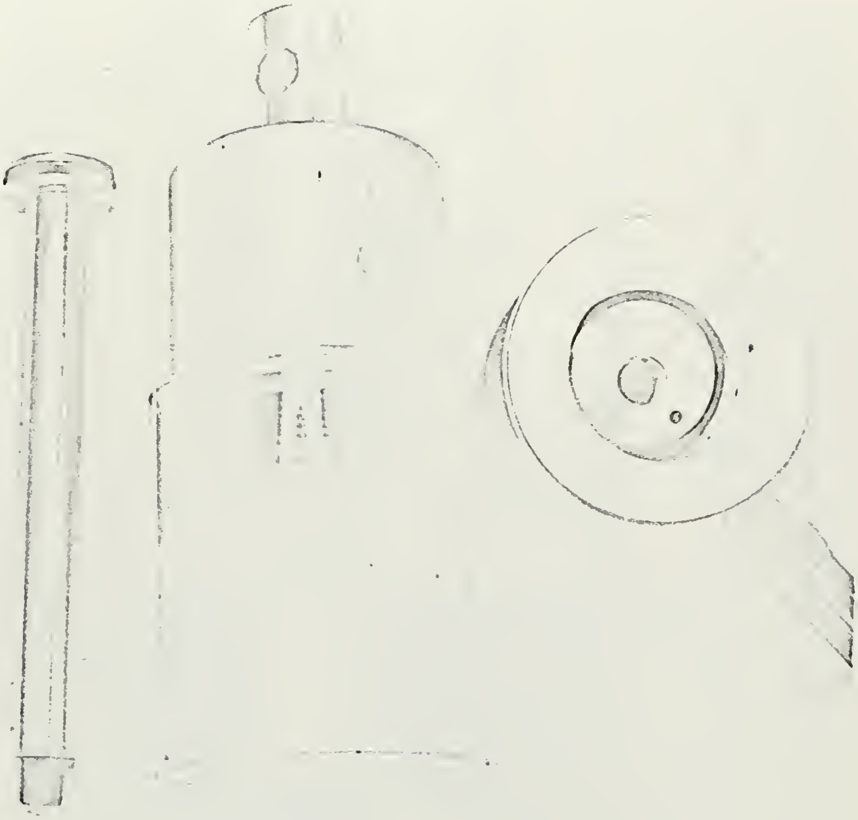

Figure 1

Instron Grip Assembly used in biaxial testing. Shown left to right, piston with high pressure O-ring seal, upper instron grip with two bleed-off ports, plexiglass shield and lower grip with hydraulic fluid inlet and high pressure O-ring.

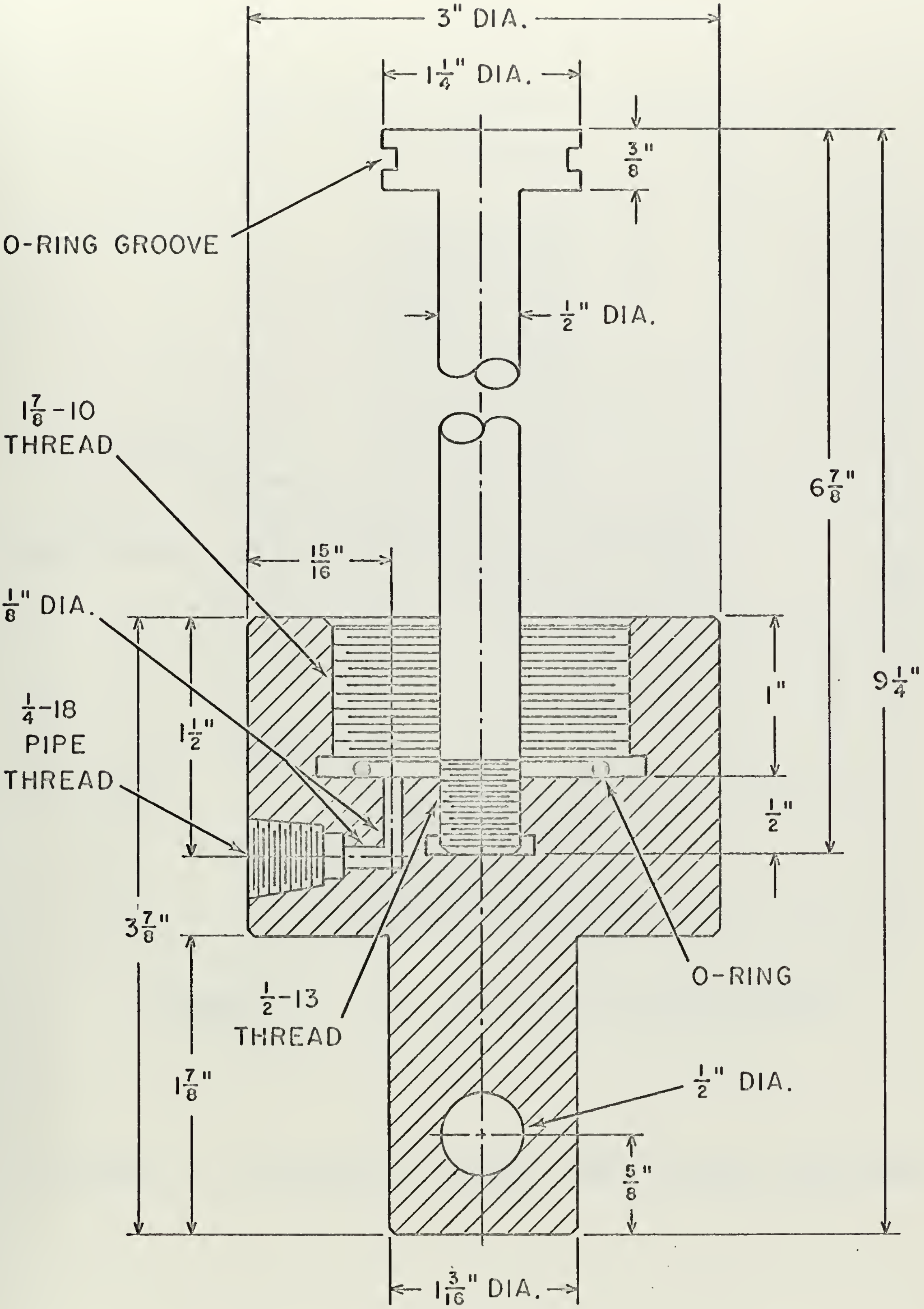

FIGURE 2. INSTRON LOWER GRIP CROSS SECTION.

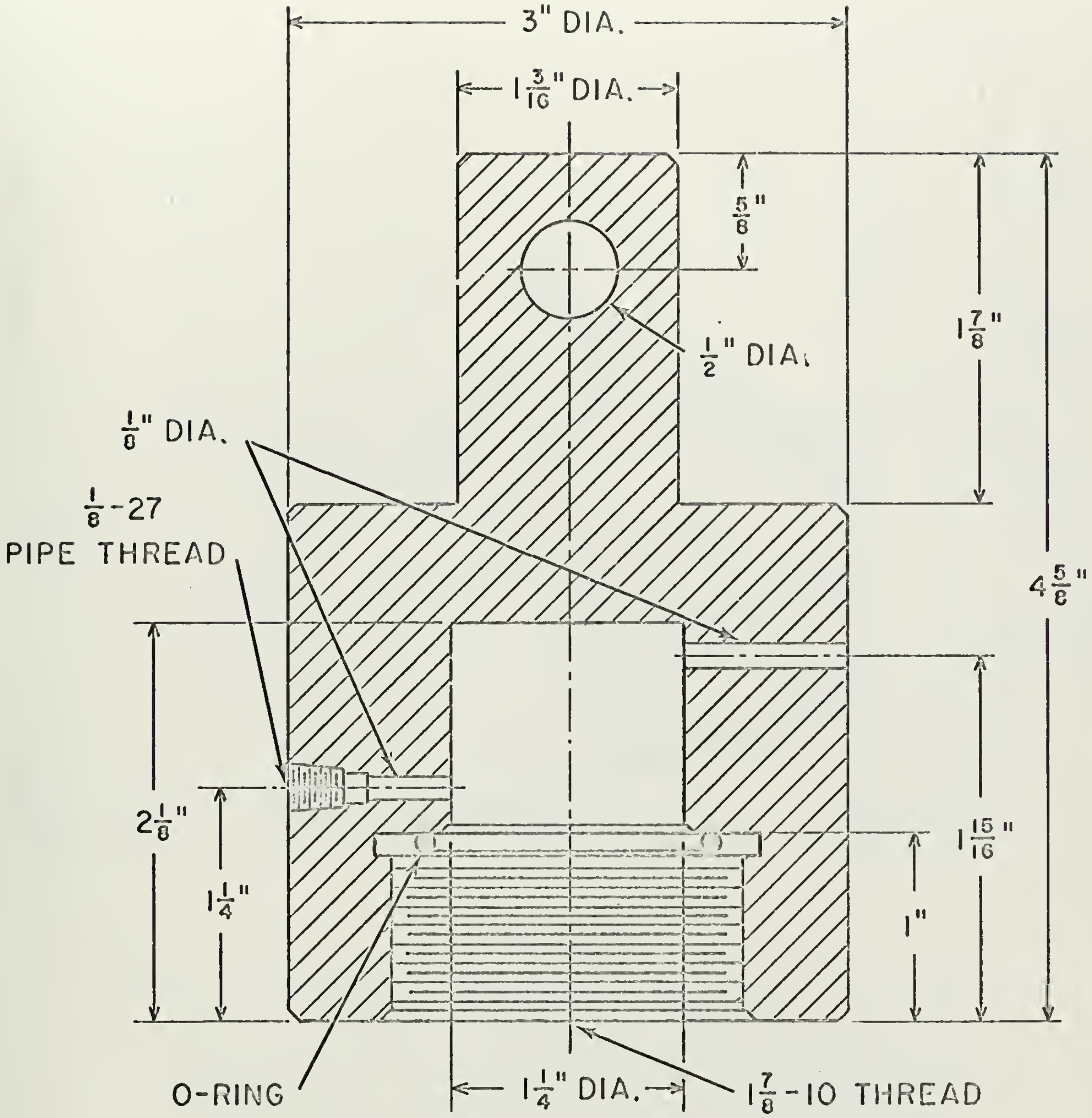

FIGURE 3. INSTRON UPPER GRIP CROSS SECTION.

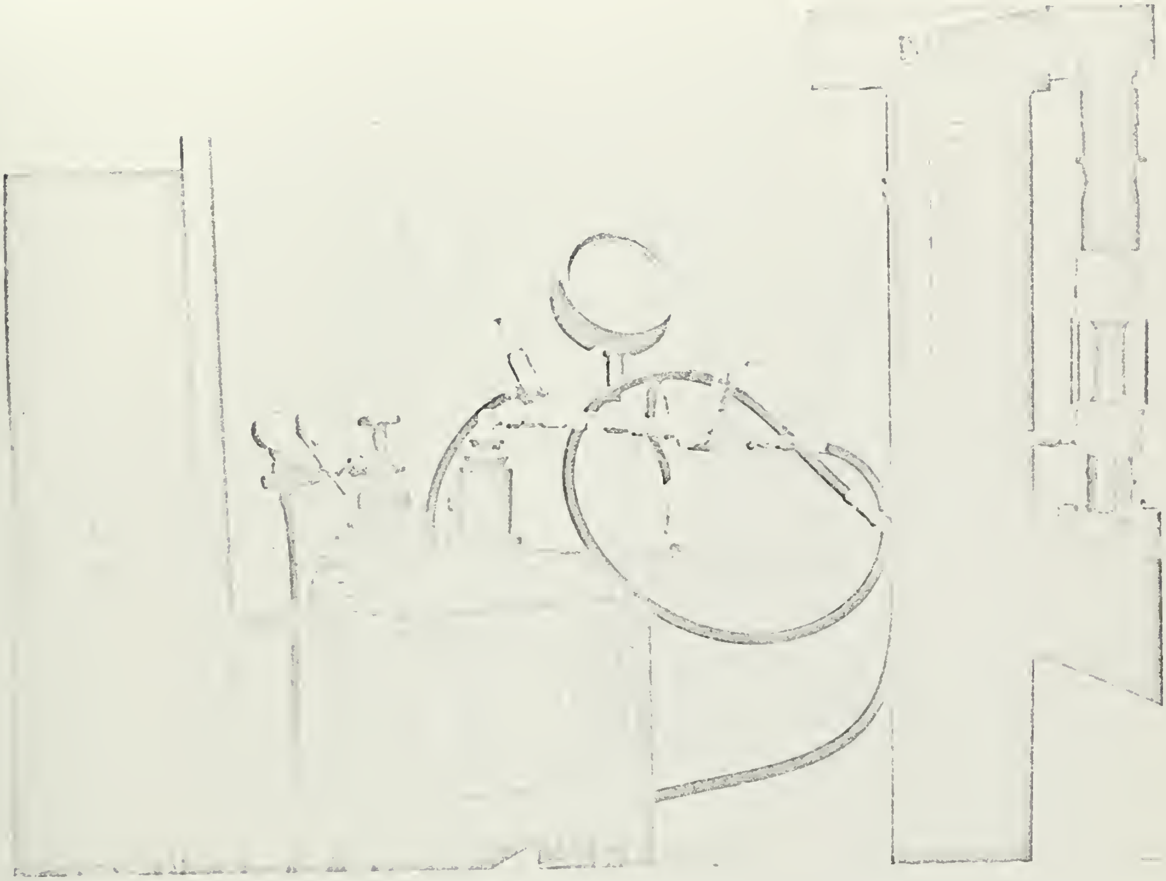

Figure 4

Biaxial testing apparatus. Shown left to right, Instron cabinet, nitrogen storage cylinder with regulator valve, hydraulic accumulator flask with valves and hydraulic pressure gauge and the Instron grips, with specimen, mounted between the crosshead and load cell of the Instron.

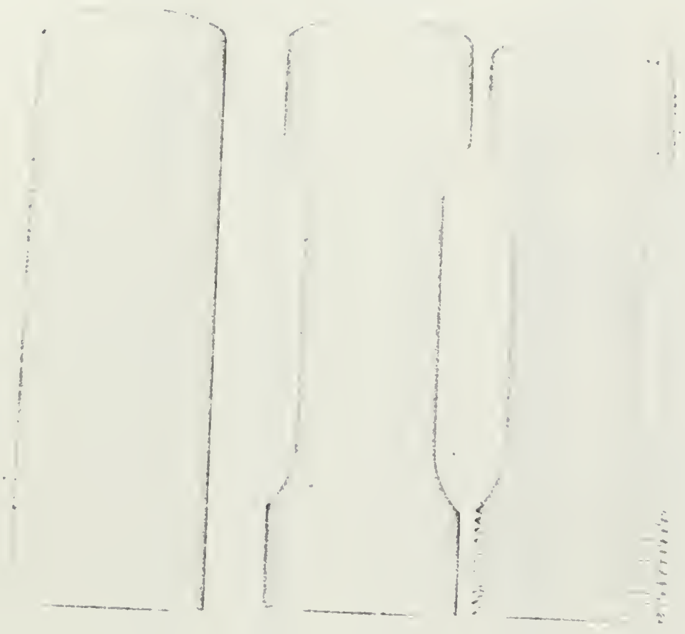

Figure 5

Biaxial specimen machining sequence. Shown left to right, hollow cylindrical casting, machined gage length and final biaxial specimen with threaded ends.

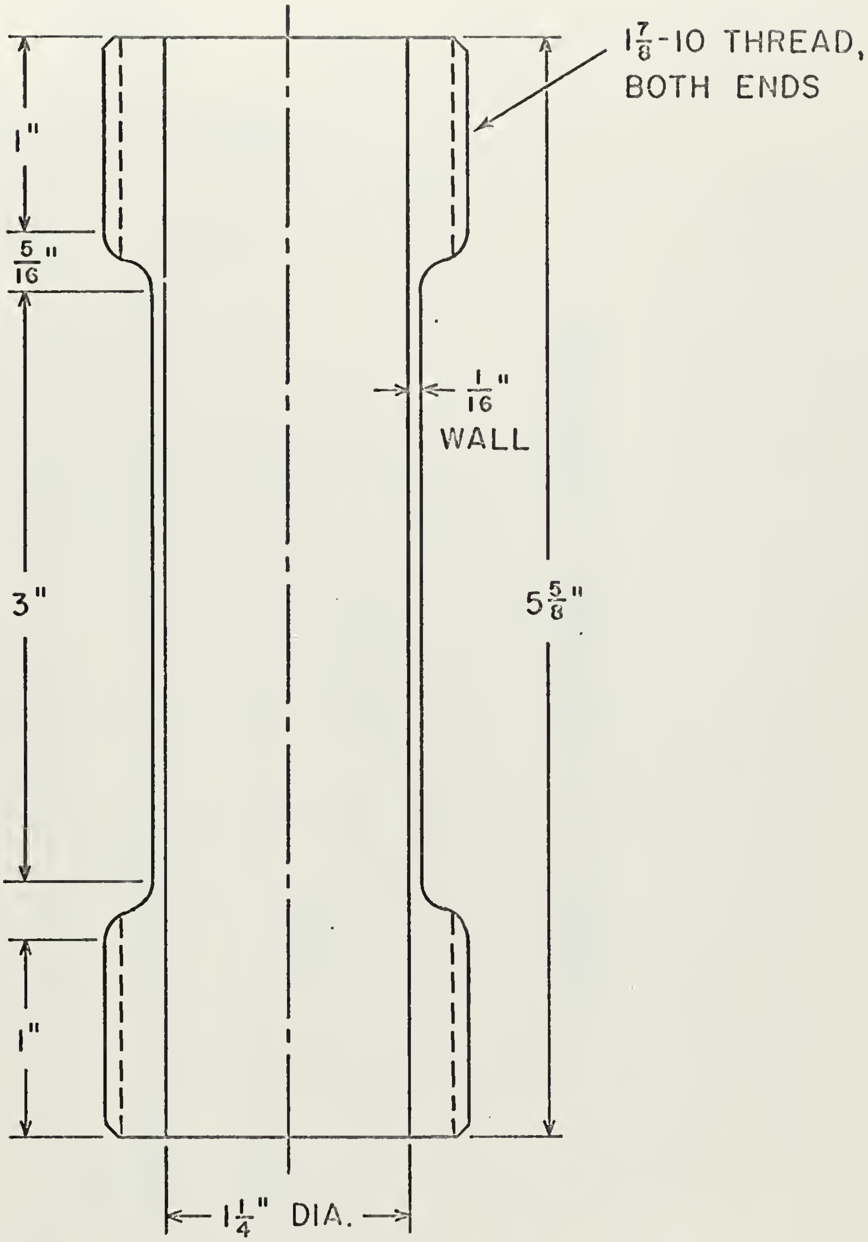

FIGURE 6. BIAXIAL SPECIMEN CROSS SECTION.

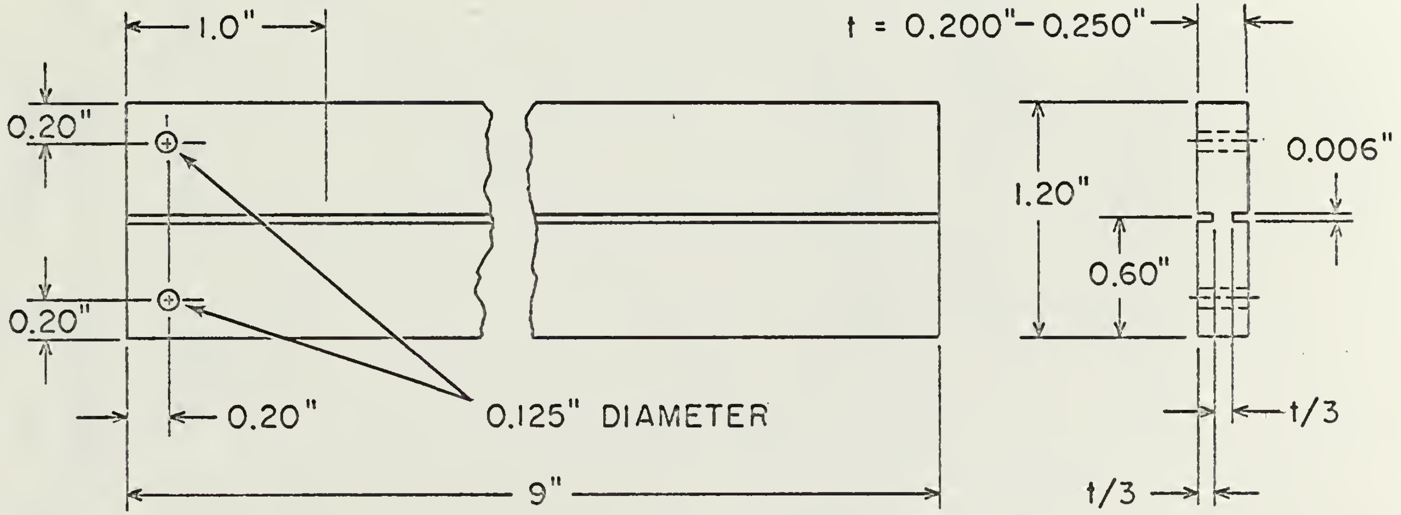

FIGURE 7. CLEAVAGE SPECIMEN.

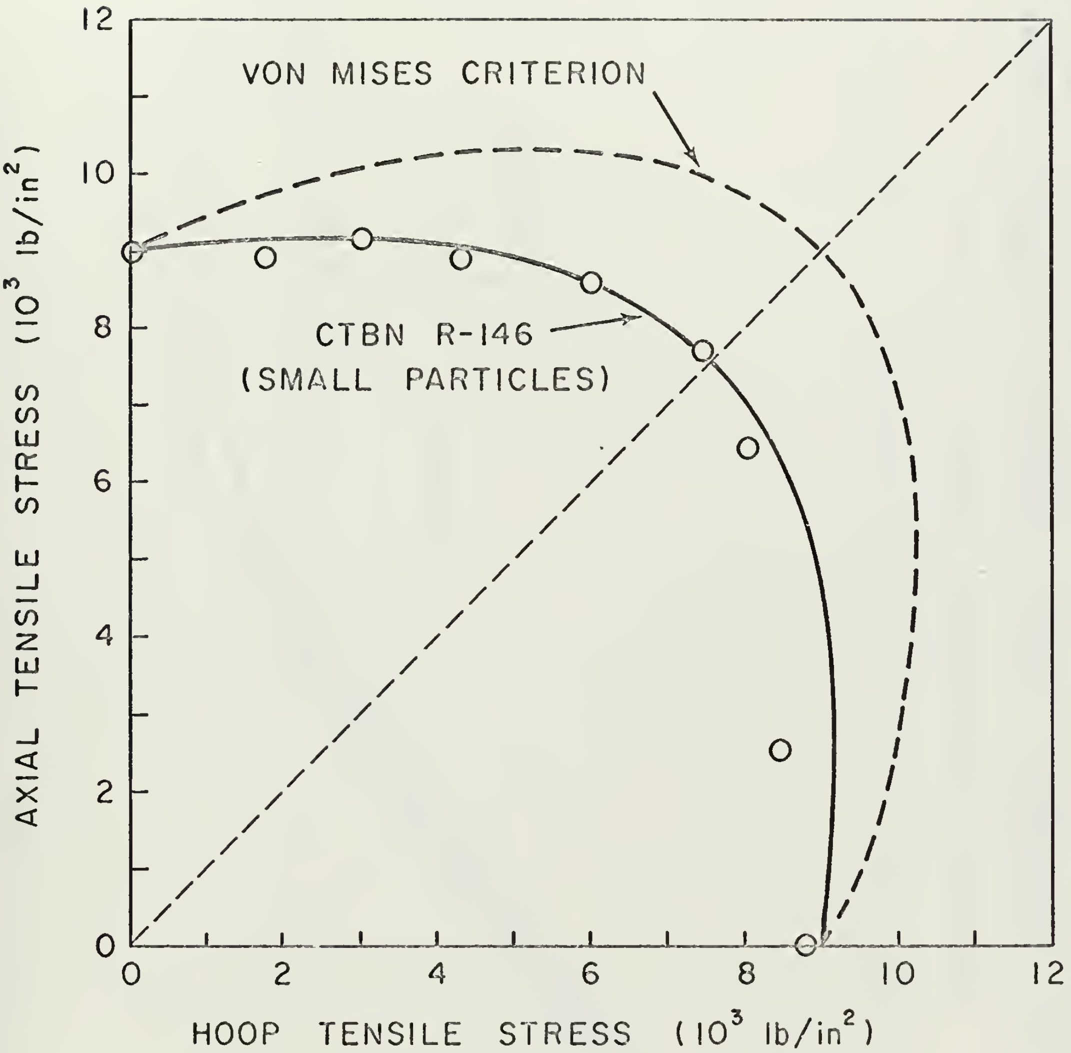

FIGURE 8. BIAXIAL SPECIMEN. AXIAL TENSILE STRESS, σ_a, vs. HOOP TENSILE STRESS, σ_h, FOR EPON 828 MODIFIED WITH CTBN R-146 (SMALL PARTICLES).

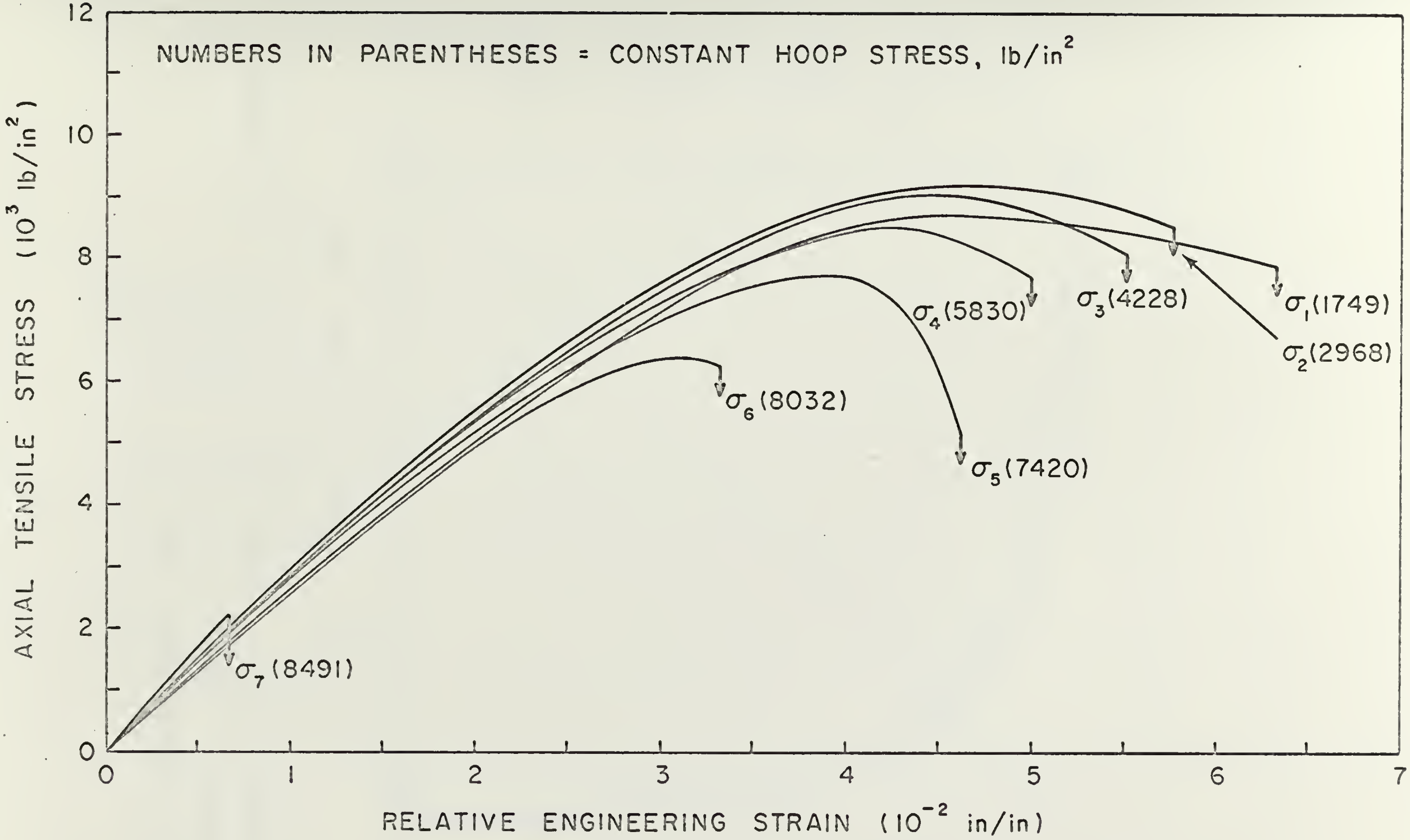

FIGURE 9. BIAXIAL SPECIMEN. AXIAL TENSILE STRESS, σ_a, vs. RELATIVE ENGINEERING STRAIN FOR EPON 828 MODIFIED WITH CTBN R-146 (SMALL PARTICLES).

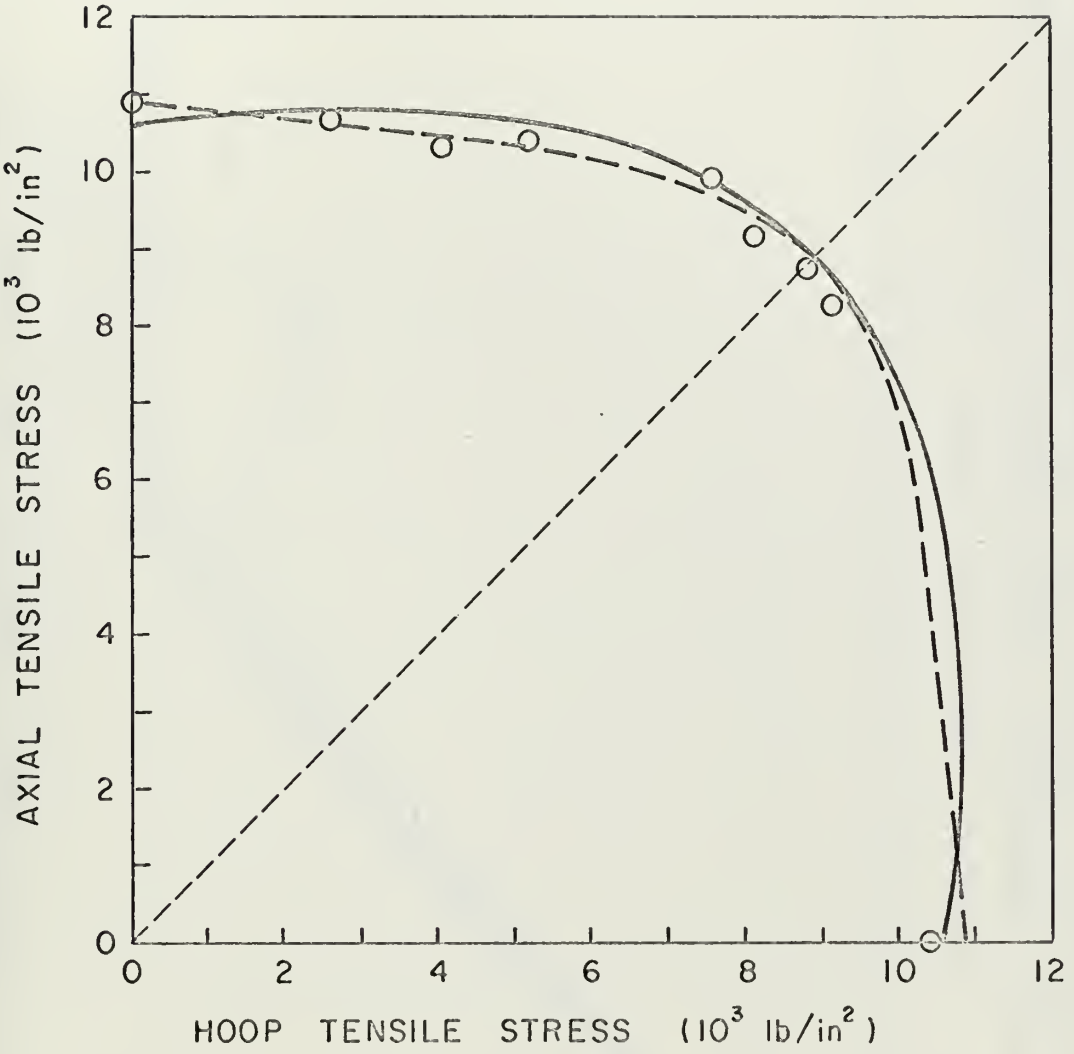

FIGURE 10. BIAXIAL SPECIMEN. AXIAL TENSILE STRESS, σ_a, vs. HOOP TENSILE STRESS, σ_h, FOR UNMODIFIED EPON 828.

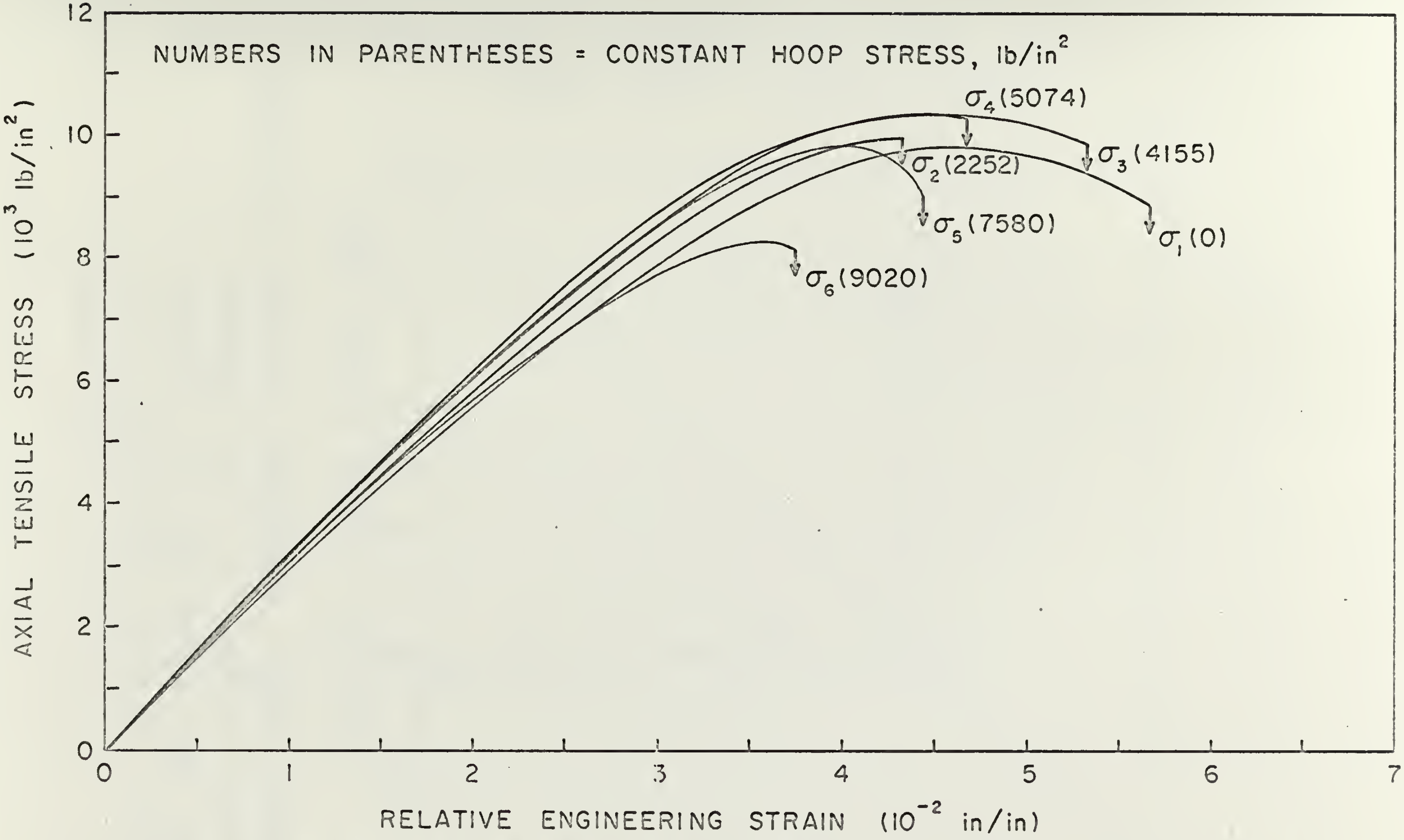

FIGURE 11. BIAXIAL SPECIMEN. AXIAL TENSILE STRESS, σ_a, vs. RELATIVE ENGINEERING STRAIN FOR UNMODIFIED EPON 828.

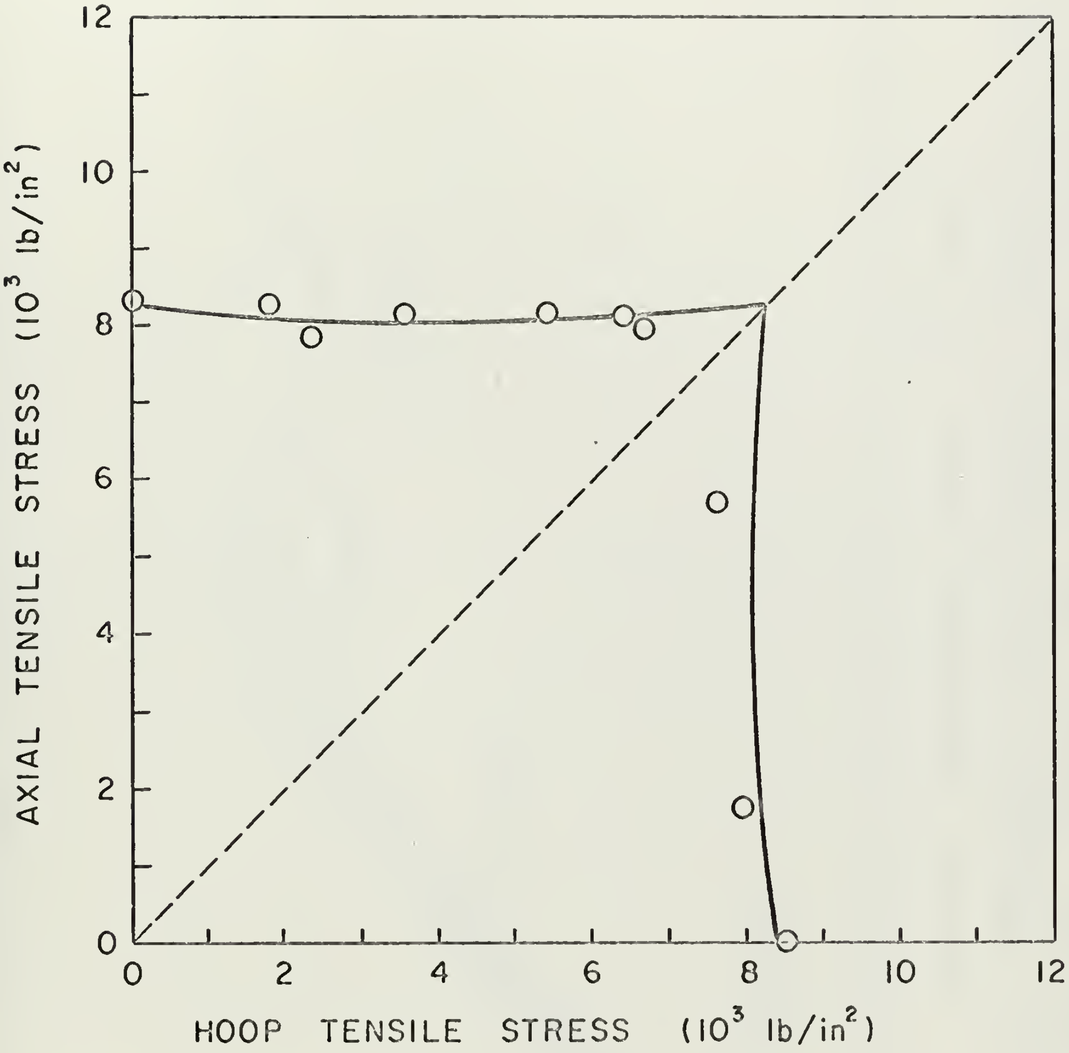

FIGURE 12. BIAXIAL SPECIMEN. AXIAL TENSILE STRESS, σ_a, vs. HOOP TENSILE STRESS, σ_h, FOR EPON 828 MODIFIED WITH CTBN R-151N (LARGE PARTICLES).

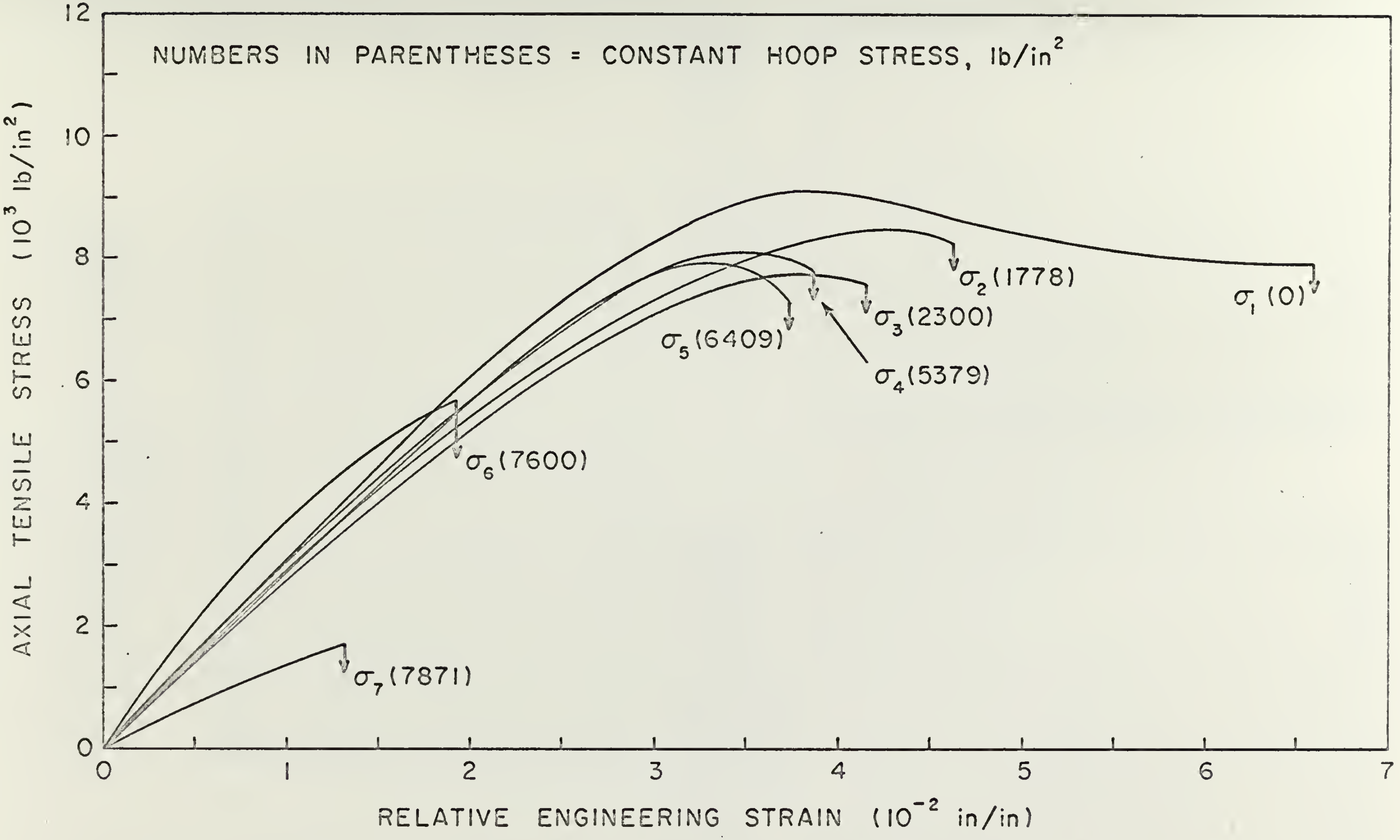

FIGURE 13. BIAXIAL SPECIMEN. AXIAL TENSILE STRESS, σ_a, vs. RELATIVE ENGINEERING STRAIN FOR EPON 828 MODIFIED WITH CTBN R-151N (LARGE PARTICLES).

Figure 14

Optical micrograph of CTBN R-151N biaxial specimen surface in reflected polarized light (138.6X)

Figure 15

Optical micrograph of CTBN R-151N biaxial specimen surface in transmitted polarized light (283.5X)

Figure 16

Optical Micrograph of CTBN R-151N Biaxial specimen surface in transmitted polarized light (562.5X)

Figure 17

Cantilever cleavage surface of CTBN R-151N cured at 74°C. At left is fast crack propogation, center is stress whitened slow crack propogation, at right is fast crack propogation.

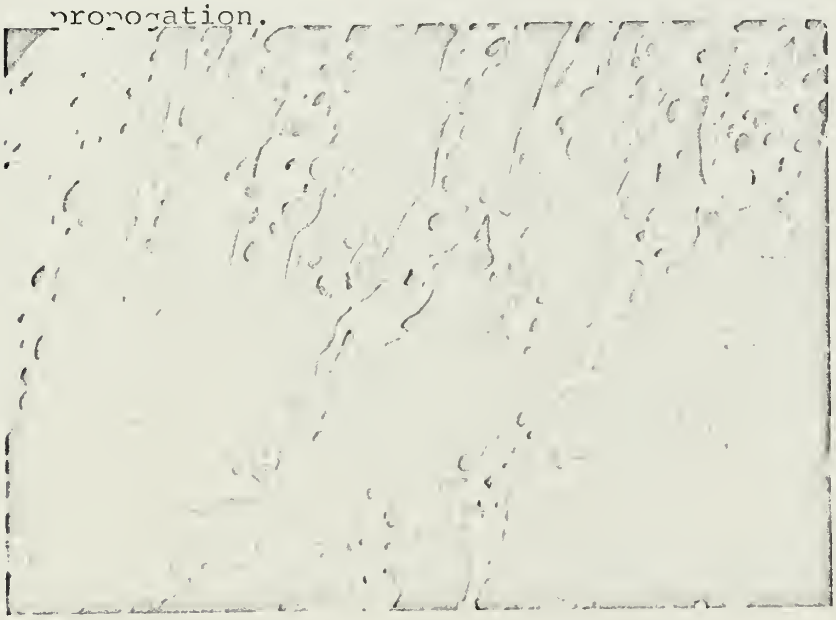

Figure 18

Cantilever cleavage surface, slow crack propogation of CTBN R-151

Figure 19

Cantilever cleavage surface of CTBN R-151N, fast crack propogation.

Figure 20

Annealed cantilever cleavage surface of CTBN R-151, slow crack propogation.

Figure 21

Biaxial specimen surface, CTBN R-151N.

Figure 22

Biaxial Specimen surface, CTBN R-151N.

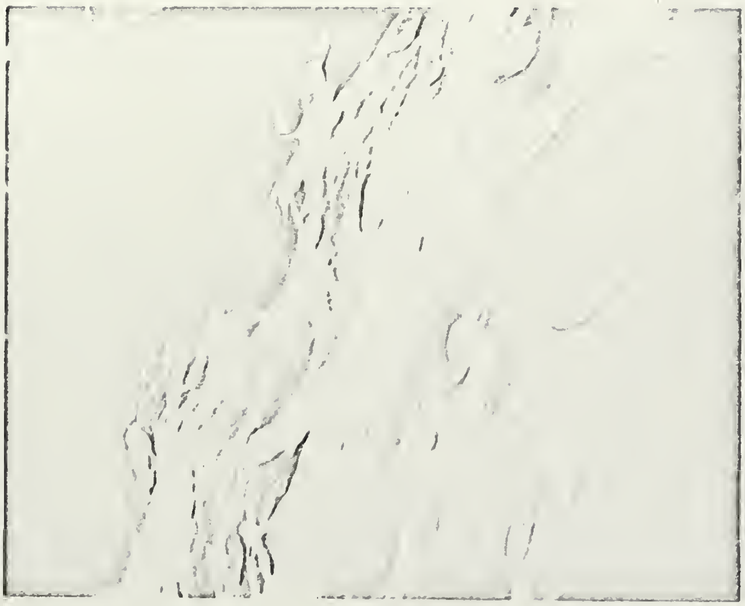

Figure 23

Biaxial specimen surface of CTBN R-151N.

Figure 24

Biaxial specimen surface of CTBN R-151N.

Figure 25

Acetone wiped surface of CTBN R-151.

Figure 26

Cantilever cleavage surface of CTBN R-146, slow crack propogation.

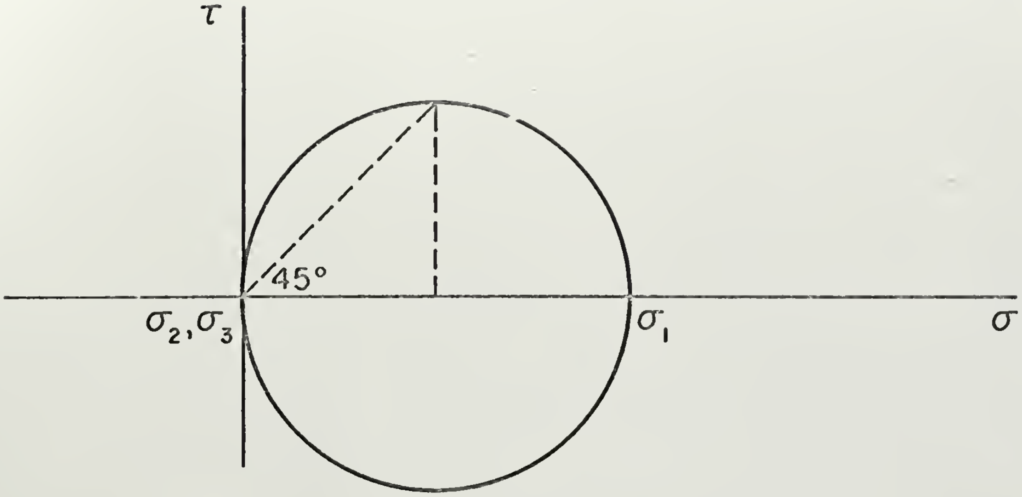

FIGURE 27. MOHR CIRCLE FOR SPECIMEN IN UNIAXIAL TENSILE STRESS; $\tau_{max} = \sigma_1/2$.

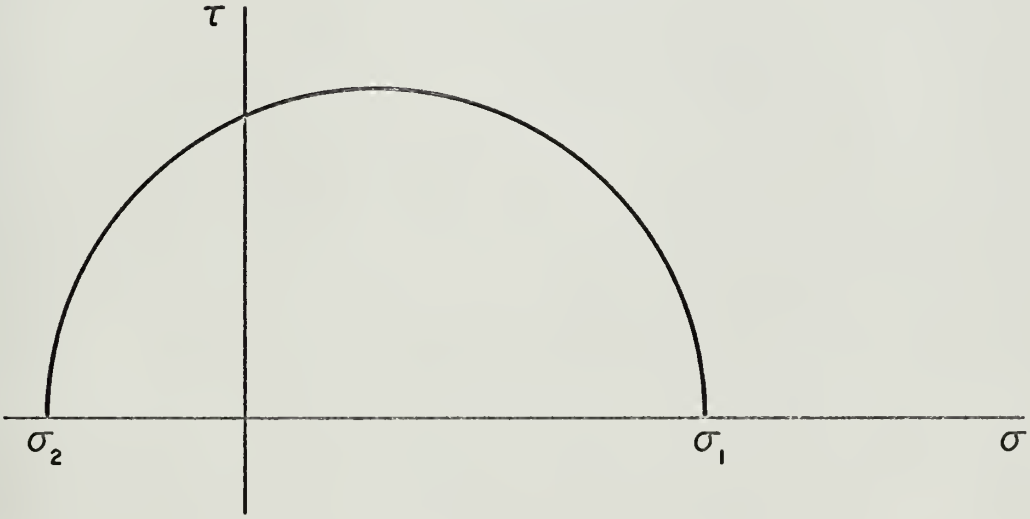

FIGURE 28. MODIFIED MOHR CIRCLE IN THE VICINITY OF A RUBBER PARTICLE FOR THE CASE WHERE σ_2 IS NEGATIVE; $\tau_{max} = (\sigma_1 - \sigma_2)/2$.

Thesis 118365
035 Oien
An investigation of biaxial stress in rubber modified plastics.
23 SEP 70 DISPLAY

Thesis 118365
035 Oien
An investigation of biaxial stress in rubber modified plastics.

thesO35
An investigation of biaxial stress in ru
3 2768 001 96942 1
DUDLEY KNOX LIBRARY